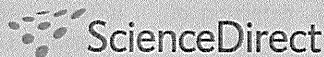
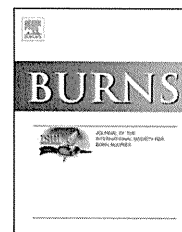


available at [www.sciencedirect.com](http://www.sciencedirect.com)journal homepage: [www.elsevier.com/locate/burns](http://www.elsevier.com/locate/burns)

## Second harmonic generation and multiphoton microscopic detection of collagen without the need for species specific antibodies

Alice C.-H. Chen<sup>a</sup>, Celia McNeilly<sup>b</sup>, Ashley P.-Y. Liu<sup>a</sup>, Christopher J. Flaim<sup>b</sup>, Leila Cuttle<sup>a</sup>, Mark Kendall<sup>b</sup>, Roy M. Kimble<sup>a</sup>, Hiroshi Shimizu<sup>c</sup>, James R. McMillan<sup>a,\*</sup>

<sup>a</sup> The Centre for Children's Burns Research, Queensland Children's Medical Research Institute, Royal Children's Hospital, The University of Queensland, Brisbane, QLD 4029, Australia

<sup>b</sup> Australian Institute for Bioengineering and Nanotechnology, The University of Queensland, Brisbane, QLD 4072, Australia

<sup>c</sup> Department of Dermatology, Hokkaido University Graduate School of Medicine, Sapporo, Japan

### ARTICLE INFO

#### Article history:

Accepted 21 March 2011

#### Keywords:

Multi-photon microscope  
Second harmonic generation  
Collagen  
Burn wound  
Scar

### ABSTRACT

High-resolution, high-contrast, three-dimensional images of live cell and tissue architecture can be obtained using second harmonic generation (SHG), which comprises non-absorptive frequency changes in an excitation laser line. SHG does not require any exogenous antibody or fluorophore labeling, and can generate images from unstained sections of several key endogenous biomolecules, in a wide variety of species and from different types of processed tissue. Here, we examined normal control human skin sections and human burn scar tissues using SHG on a multi-photon microscope (MPM). Examination and comparison of normal human skin and burn scar tissue demonstrated a clear arrangement of fibers in the dermis, similar to dermal collagen fiber signals. Fluorescence-staining confirmed the MPM-SHG collagen colocalization with antibody staining for dermal collagen type-I but not fibronectin or elastin. Furthermore, we were able to detect collagen MPM-SHG signal in human frozen sections as well as in unstained paraffin embedded tissue sections that were then compared with hematoxylin and eosin staining in the identical sections. This same approach was also successful in localizing collagen in porcine and ovine skin samples, and may be particularly important when species-specific antibodies may not be available. Collectively, our results demonstrate that MPM SHG-detection is a useful tool for high resolution examination of collagen architecture in both normal and wounded human, porcine and ovine dermal tissue.

Crown Copyright © 2011 Published by Elsevier Ltd and ISBI. All rights reserved.

## 1. Introduction

Multi-photon microscopy (MPM) is a nonlinear optical phenomenon that provides intrinsic optical sectioning of a

specimen, and can provide high-resolution, high-contrast three-dimensional views of live cell and tissue architecture. Several extracellular matrix (ECM) components and key endogenous biomolecules can be visualized *in situ* without the need for tissue processing and staining, exogenous

\* Corresponding author at: The University of Queensland, The Centre for Children's Burns Research, Queensland Children's Medical Research Institute, Level 4 Foundation Building, Royal Children's Hospital, Brisbane, QLD 4029, Australia. Tel.: +61 7 3636 9069; fax: +61 7 3365 5455.

E-mail address: [j.mcmillan@uq.edu.au](mailto:j.mcmillan@uq.edu.au) (J.R. McMillan).

0305-4179/\$36.00. Crown Copyright © 2011 Published by Elsevier Ltd and ISBI. All rights reserved.

doi:10.1016/j.burns.2011.03.013

antibody labeling or fluorophores. These include the auto-fluorescence from reducing coenzyme NAD(P)H, flavoproteins, keratin, melanin, and elastin [1]. In addition, detection of second-harmonic generation (SHG), the non-absorptive frequency changes in an excitation laser line can also be performed using MPM. SHG is a nonlinear optical effect that results in an emission wavelength that is half the excitation wavelength. Myosin, tubulin and collagen polymeric proteins have previously been studied using SHG [2-4]. Recent studies have used SHG signals to look at various skin disorders [1,5], and even immune cell migration in the skin [6]. Furthermore, it has also been shown to be a powerful tool in tissue engineering and can be used to monitor drug delivery [7,8].

In human skin, collagen makes up 70% of the dry weight of the dermis. Dermal fibroblasts are responsible for regulating the steady state synthesis of collagen deposition in normal skin. Several matrix metalloproteinases (MMPs 1, 2, 3, 8, 9, 13, 18) are responsible for collagen degradation, hence maintaining collagen-tissue equilibrium [9]. The balance between collagen production by (myo-)fibroblasts and collagen degradation by matrix metalloproteinases determines the precise collagen bundle size and hence dermal thickness during the process of post wounding dermal remodeling. After massive burn injury, granulation tissue formation and dermal remodeling takes place to fill and repair the damaged tissue. With deep dermal burns, this often results in an unsightly, raised hypertrophic scar. The scars are usually active for more than six months after injury, and mature after 18 months [10,11]. However, the orientation and distribution of collagen fiber arrangement at different time points after burn and in the pathophysiology of hypertrophic scar formation is still unclear.

It is well understood that hypertrophic scars have different collagen organization compared to normal skin, and that collections of parallel fibers and collagen nodules can be observed at different stages of scarring [12]. Several studies have been carried out to observe collagen architecture in hypertrophic scars, however many of the methods for detecting the presence of dermal collagens have been costly, time consuming and involved immunohistochemical antibody staining on tissue sections. In addition, studies using animal models often face difficulties finding species-specific antibodies, and there is also a need for *in vivo* imaging techniques to be developed. This study attempted to use an alternative higher-resolution microscopic method to assess collagen fiber arrangements in control and burn scar skin

tissues. We examined human, porcine and ovine normal skin sections and compared these to dermal tissue at several different stages after burn using MPM based on SHG, and determined that MPM detection of SHG is a powerful tool for examination of collagen architecture in skin.

## 2. Materials and methods

### 2.1. Sample preparation

This research has been approved by the Royal Children's Hospital and Health Services District Human Research Ethics Committee and all studies were performed in accordance with the Helsinki declaration. Normal Human and scar tissue sections were collected from scar excision surgeries in the Royal Children's Hospital in Brisbane, Australia. Two surgically removed human foreskin tissues were also collected to represent normal human tissues (Table 1). Both donors were less than 12 months of age. The scar tissue donors were Asian girls aged 10 and 11 with burn scar tissue collected from the upper aspect of the foot and right thigh respectively approximately three years after the initial burn. All skin tissues collected were (1) fixed in 4% formalin, embedded in paraffin, and (2) embedded in OCT (embedding medium for frozen tissue to ensure Optimal Cutting Temperature) and snap frozen in liquid nitrogen, with sections cut at 5 microns ( $\mu\text{m}$ ). Porcine normal and scar skin sections used in this experiment were first described by Cuttle et al. [13]. Burns were created on Large White juvenile pigs of approximately 8 weeks of age using 92 °C water for 15 s. A deep dermal partial thickness burn was created, with hypertrophic scarring observed after 99 days. Hypertrophic scar and normal skin samples were collected and fixed in 4% formalin, then embedded in paraffin. Skin samples of two pigs were used in this study. Ovine skin sections used in this experiment were first described by Fraser et al. [14]. Burns were created on Merino ewe fetuses at 80 days gestation using 66 °C water for 7 s and the tissue collected at 60 days post-burn. Merino ewe lambs were burned with 82 °C water for 10 s at 28-30 days of age and the tissue was collected 1 day later. Burn and normal skin samples were collected at several time points and fixed in 10% formalin then embedded in paraffin. Skin samples of three ovine fetuses and two ovine lambs were used in this study. All samples were examined in duplicate.

**Table 1 – The origin, age and location of tissues used in this study.**

Sample	Species	Age	Time after burn	Gender	Body site	Ethnic background/species type
Normal 1	Human	Less than 1 year	–	Male	Foreskin	Caucasian
Normal 2	Human	Less than 1 year	–	Male	Foreskin	Caucasian
Scar 1	Human	10 years	40 months	Female	Ankle	Asian
Scar 2	Human	11 years	44 months	Female	Right thigh	Asian
Porcine normal/porcine scar	Porcine	22 weeks	99 days	Female	Right flank	Large White pig
Fetus normal/fetus burn	Ovine	140 days fetal gestation (term = 145–150 days)	60 days	–	Flank	Merino ewes
Lamb normal/lamb burn	Ovine	4 weeks	1 day	Male	Lower abdomen	Merino ewes

## 2.2. Multiphoton microscopy

A Zeiss 510 Meta NLO multi-photon microscope (Zeiss, North Ryde, NSW, Australia) was used to detect the SHG signal from both frozen sections and paraffin sections to determine the optimal spectral parameters for SHG excitation and signal collection for each technique (frozen or paraffin), species (human or pig) and specimen (normal skin or burn scar) types. Previous studies have used an excitation wavelength of 800–860 nm to detect collagen SHG [15–18], therefore here we used the BP 390–465 filter (collection wavelength of 390–465 nm) to cover the excitation wavelengths from 780 to 930 nm. Systematic checking of each excitation wavelength for optimal collagen visualization was performed by preliminary excitation wavelength screening at 10 nm intervals ranging from 790 nm to 920 nm. The 20× objective lens was used throughout this experiment (SHG and H&E visualizations). In order to confirm that the SHG signal detected was in fact

specific for collagen, sequential SHG and Alexa488 fluorescent signals from immunohistochemically stained tissue sections were collected. Colocalization of SHG signal and Alexa488 was performed using the optimally determined SHG excitation/emission wavelength combination together with a second channel collecting the 500–550 nm emission from Alexa 488 (excited by a 488 nm laser). Zeiss AIM software was used to visualize the images. After SHG imaging both cryostat and paraffin sections were stained using routine hematoxylin and eosin (H&E) staining methods with acetone pre-treatment for cryostat sections [19].

## 2.3. Indirect immunofluorescent staining

For collagen I and fibronectin staining on frozen sections, slides were incubated in 10% goat serum (Millipore, CA, USA) blocking solution for 30 min, then incubated in a 1:100 dilution of collagen I monoclonal antibody ([COL-1] ab6308 Abcam,

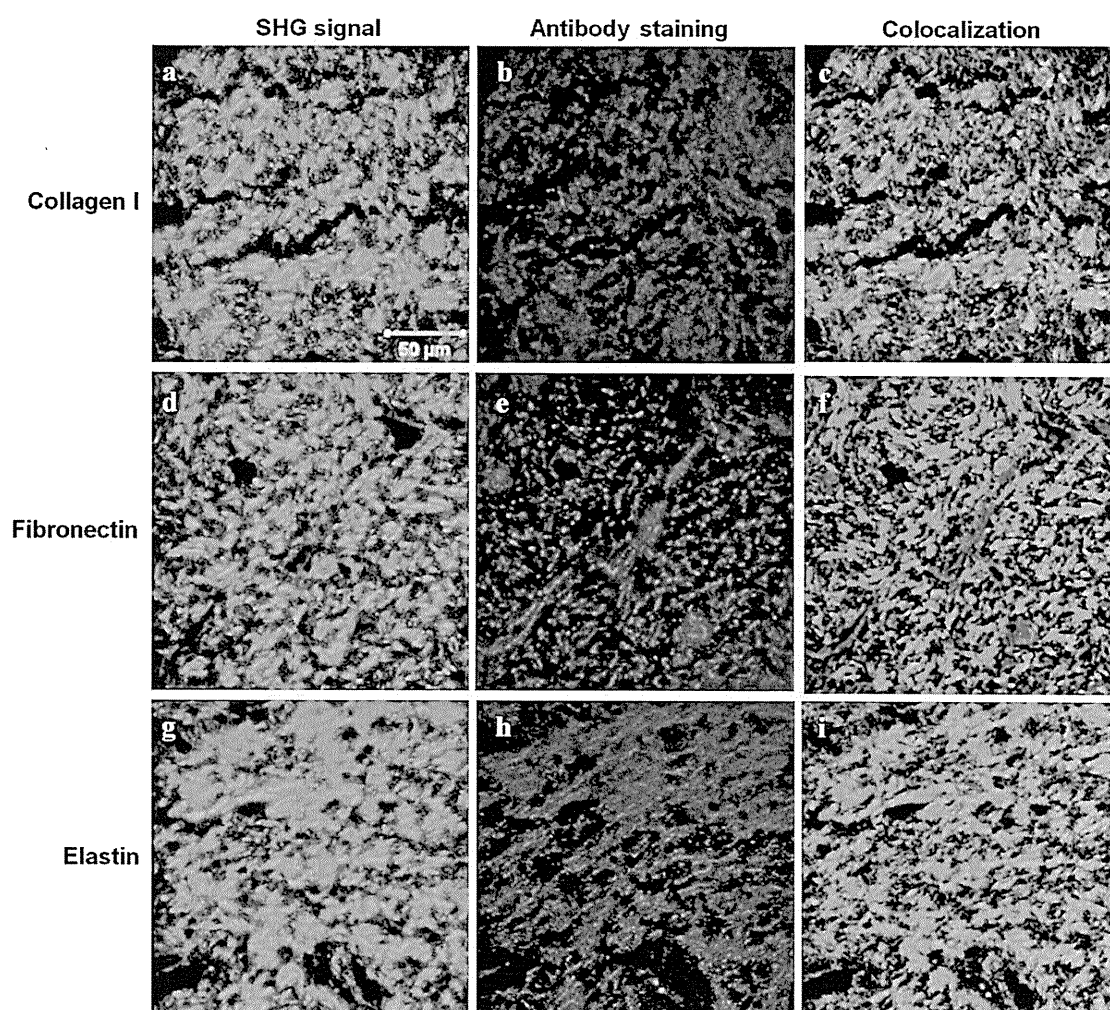


Fig. 1 – Co-localization of secondary harmonic image generation (SHG) and collagen I-, fibronectin- and elastin-antibody labeled human tissue sections show that the SHG signal closely co-localizes with collagen I-antibody staining, but not fibronectin or elastin. (a and d) SHG visualized on a frozen human Normal 1 tissue section, (g) SHG visualized on paraffin-embedded human Normal 1 tissue section, (b) collagen I-antibody labeled Alexa488 signal, (e) fibronectin-antibody labeled Alexa488 signal, (h) elastin-antibody labeled Alexa488 signal, and (c, f, and i) co-localization of SHG signal and antibody labeling.

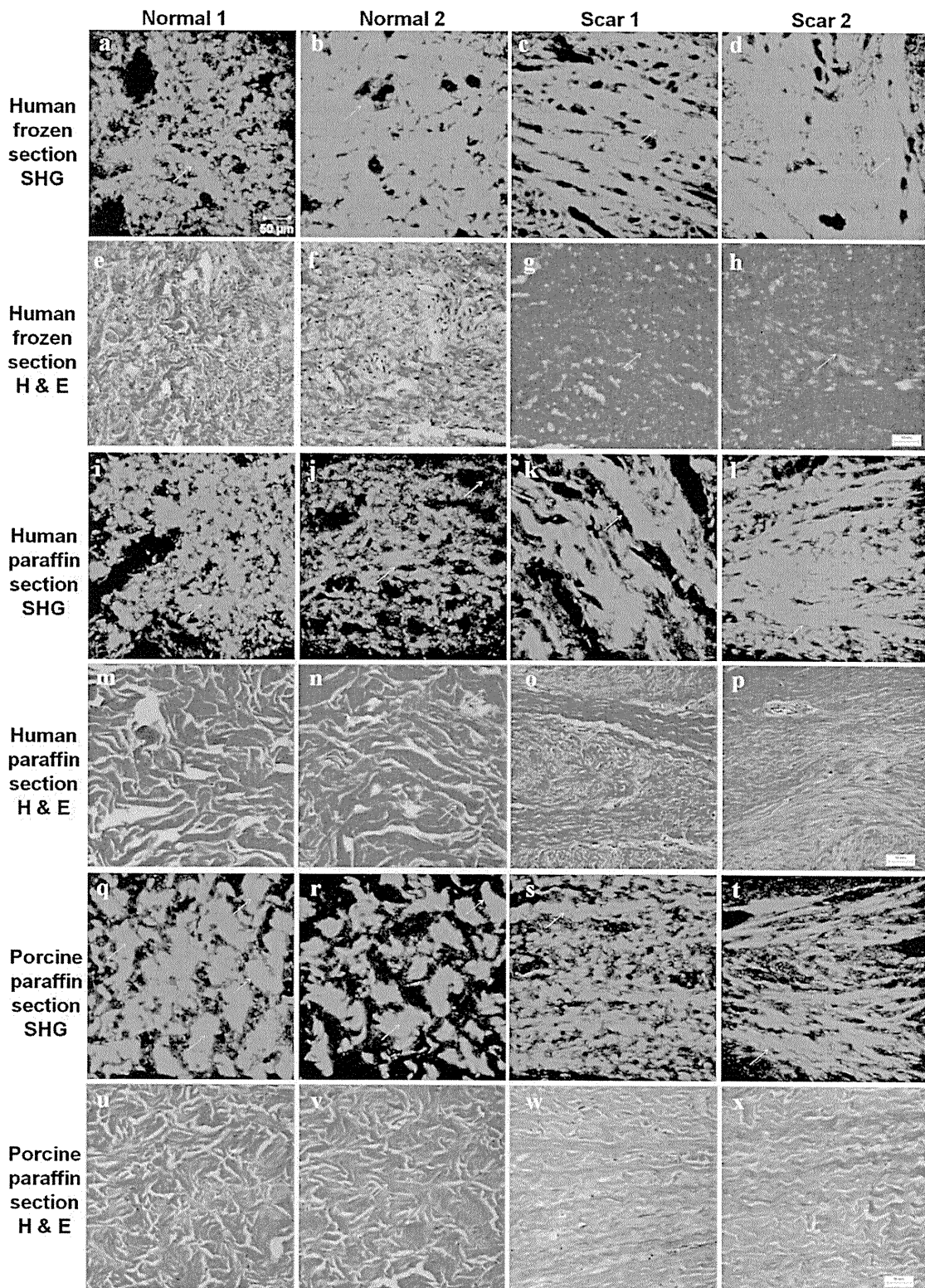


Fig. 2 - Human (a-p) and porcine skin (q-x) collagen architecture visualized using secondary harmonic image generation (SHG) and hematoxylin and eosin staining. All images were taken with the same microscope configuration/magnification to compare the differences in signal intensity and collagen arrangement between normal skin and scar tissue. The arrows in the control samples indicate the basket-weave arrangement in normal tissue, and highlight the elongated, wavy, undulating parallel collagen fibers observed in scar tissues. Collagen fiber bundles in H&E stained and SHG-visualized paraffin embedded sections

Cambridge, MA, USA) [20] or neat fibronectin supernatant monoclonal antibody HFN7.1 (DSHB, TX, USA) [21] at room temperature for 1 h in a humid atmosphere. After three washes in 0.1 M Dulbecco's phosphate buffered saline (PBS, five minutes per wash), slides were incubated in 1:500 Alexa Fluor 488 goat anti-mouse IgG antibody (Invitrogen, CA, USA) for 30 min at room temperature in a humid atmosphere in the dark. Microscope slides were washed three times in PBS, in distilled water and then coverslip mounted with Vectashield containing the nuclear staining agent, DAPI (1.5  $\mu\text{g}/\text{ml}$ ) (Vector Laboratories, Burlingame, CA, USA), and the coverslip edges sealed with non-fluorescent nail polish [22].

For elastin staining, as this antibody did not work in frozen sections, paraffin sections were dewaxed in xylene and processed through a descending ethanol series of washes, followed by trypsinization at 37 °C for 30 min using 0.2% trypsin (Gibco, CA, USA). Antibody permeabilization using 0.1% Triton X-100 (Merck, Australia) in PBS was performed at room temperature, incubated for 10 min with subsequent 30 min blocking in 10% normal goat serum (Millipore, CA, USA) in permeabilization solution at room temperature. Sections were incubated in 1:500 dilution monoclonal anti-elastin clone BA-4 (Sigma-Aldrich, MO, USA) [23] overnight at 4 °C. After three washes in PBS (five minutes each wash), slides were incubated in 1:500 Alexa Fluor 488 goat anti-mouse IgG antibody (Invitrogen, CA, USA) for 30 min at room temperature in the dark. Slides were then washed three times in PBS, then mounted with Vectashield with DAPI (Vector Laboratories, Burlingame, CA, USA) and the coverslips sealed with nail polish.

### 3. Results

To assess whether MPM is a viable alternative microscopic method to examine collagen deposition in control and burn scar tissues, we examined human normal skin and scar tissue using the MPM to detect SHG. Our results demonstrated that collagen SHG is best detected with lowest background noise at an excitation wavelength of 860 nm and an emission wavelength of 390–465 nm (data not shown). The localization of this putative collagen-SHG pattern was further compared to other dermal matrix components and was compared by dual channel colocalization with immunostaining using collagen I-, fibronectin- and elastin-antibody labeled tissue sections. The detected collagen-SHG signal showed a similar basket-weave arrangement pattern to collagen I antibody staining from normal human skin tissue (Fig. 1a and b), however the images did not completely overlap (Fig. 1c). Conversely, the putative collagen-SHG signal showed a completely different pattern when compared to fibronectin and elastin staining (Fig. 1f and i), with fibronectin demonstrating a finely organized nested pattern especially immediately below the epidermis (Fig. 1e), and elastin staining showed threads of thin fibers aligning in

the same direction, parallel or perpendicular to the epidermis (Fig. 1h).

Two human control tissue samples and two human hypertrophic scar tissue samples were tested for SHG visualization and comparison with H&E staining at the optimal excitation wavelength of 860 nm, with an emission/collection wavelength of 390–465 nm. Collagen architecture in normal human dermis and burn hypertrophic scar tissue could be detected in both frozen (Fig. 2a–d) and paraffin sections (Fig. 2i–l) with similar signal intensity, however clearer collagen architecture was observed in the fixed paraffin-embedded sections (Fig. 2i–l). Collagen fibers in control foreskin sections were in a randomly but relatively loosely organized basket-weave-like arrangement, while scar tissue collagen fiber bundles comprised typically long fibers aligned in parallel or in an undulating pattern. Comparison with H&E stained cryostat and paraffin embedded sections confirmed the differences in collagen organization and packing observed by SHG between control and scar tissue. Comparison of H&E and SHG staining clearly demonstrated the higher density of collagen bundle packing in the scar samples in both cryostat (Fig. 2a–d versus e–h) and paraffin sections (Fig. 2i–l versus m–p). In general, SHG showed superior visualization of compacted collagen in bundles and the higher bundle density in human and porcine scar tissue compared to H&E stained sections. Furthermore, SHG provides significant improvements in collagen fiber resolution (see Fig. 2c and d, k and l, and s and t) that would allow clearer 3D image collection with the added benefit of ease of tissue preparation. Although the twisted or wavy characteristics of hypertrophic scar dermal collagen fibers were clearly observed in both scar sections, using both techniques (see arrows in Fig. 2k and o) no collagen nodules were visualized in these samples using either SHG or H&E visualization techniques.

The same approach was repeated using control porcine and hypertrophic scar paraffin-embedded sections to determine if different species exhibit similar optimal wavelengths for collagen SHG signal detection (see Fig. 2q–t). Our results show that porcine collagen SHG was best detected at excitation wavelength of 860 nm and an emission wavelength of 390–465 nm, which was identical to the detection of human dermal collagen (data not shown). Control porcine paraffin-embedded dermal tissue sections exhibited a stronger SHG signal intensity over the length of the shorter fibers (arrows in Fig. 2q and r) compared to scar tissue sections (Fig. 2s and t). Similar to human collagen architecture, control porcine dermis also demonstrated a basket-weave arrangement, while scar tissue exhibited extended, long wavy collagen fibers aligned in parallel with the epidermis (Fig. 2s and t). Again, H&E stained paraffin embedded sections confirmed the differences observed using SHG in collagen bundle distribution, length and packing between pig control and scar tissue samples.

**exhibited identical distribution, length and packing patterns between human and porcine control and scar tissue samples. However, upon closer comparison SHG visualization exhibited increased resolution and clarity of individual collagen bundles, especially in scar tissue from all species examined (c and d, k and l, and s and t).**

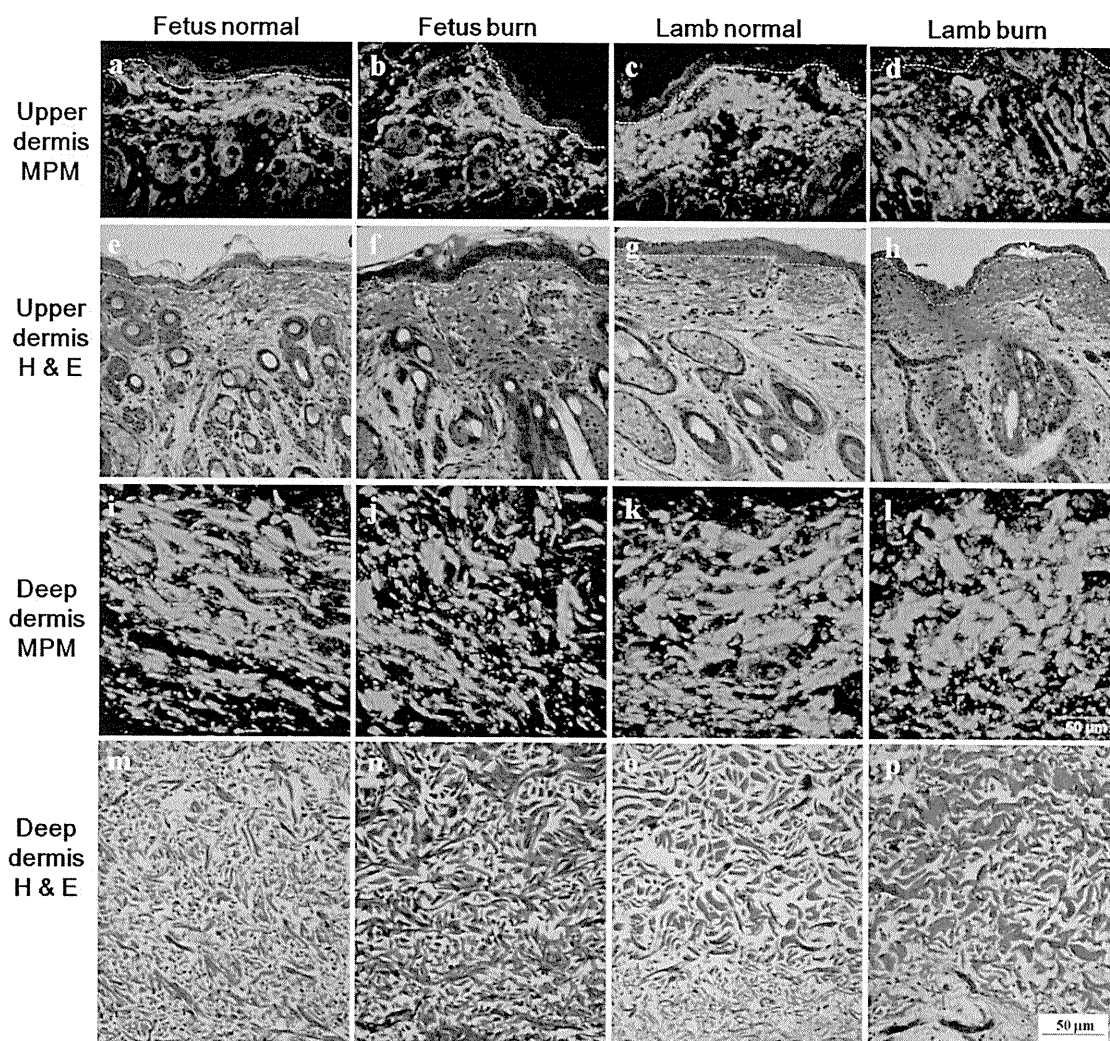


**Fig. 3 – Ovine fetus and lamb skin collagen architecture visualized using secondary harmonic generation (upper dermal a–d; lower dermal staining i–l) and hematoxylin and eosin staining (upper dermal e–h; lower dermal staining m–p) in paraffin embedded sections. All images were taken with the same microscope configuration/magnification to compare the differences in signal intensity and collagen distribution arrangement between normal skin and skin after burn. The upper dermal field of view is predominantly comprised of wool follicles with a decreased presence of collagen lower in the mid-dermal tissue. The dashed lines indicate the epidermal-dermal junction with one figure showing epidermal separation after burn wounding (asterisk in h). The H&E stained paraffin embedded sections confirmed the more subtle differences observed using SHG in collagen bundle distribution, length and packing between ovine control and burn tissue samples.**

Ovine collagen fibers were also successfully detected in both normal and burn tissue using the same MPM excitation and emission detection settings (Fig. 3). Thin collagen fibers were detected in the papillary dermis (just beneath the dashed lines Fig. 3a and b) of ovine normal control fetal tissue at 140 days gestation (term is 145–150 days) and fetal burn tissue after 60 days post-wounding normal control as well as in lamb tissue (Fig. 3c and d). Thick, SHG-bright collagen bundles were detected in both normal and burn tissues in fetal and lamb deep dermis that correlated with more eosinophilic collagen bundles in H&E sections of burn tissue (Fig. 3m and o versus n and p). Unlike human and porcine

normal skin, the collagen architecture in ovine deep dermis showed relatively longer collagen bundles parallel-aligned in a wavy pattern, but the long, continuous parallel collagen architecture seen in human and porcine scar tissue was not observed in either the adult or fetal ovine tissue. Ovine fetal deep dermis at 60 days post burn demonstrated similar looking collagen bundles to normal control fetal skin (Fig. 3i versus j), however in contrast the collagen bundles were less regularly aligned in parallel. In addition, at 1 day after burn, thick collagen bundles were still visualized in the lamb acute burn deep dermis, but in a much shorter and curled form (Fig. 3i and p).

#### 4. Discussion

Second harmonic generation detection using MPM has been widely used in various dermatological studies in the last few years [15,17,18,24]. It is a non-invasive, high resolution and high contrast laser microscopic technique that allows observation of tissue architecture, identification of skin pathology, and monitoring of drug delivery. Many dermatological studies often require immunohistochemical staining to observe different compartments of skin structure, and these methods include the most commonly used hematoxylin and eosin staining, Masson's Trichrome staining and Sirius red staining viewed using various forms of light microscopy. Antibody-labeled tissue sections or cells viewed by fluorescent or confocal laser microscopy are also frequently used to detect the distribution of specific proteins during molecular trafficking. Transmission electron microscopy can give a high magnification ultrastructural view of the tissue structure, however it is a very slow and time consuming method. Most of these methods require immunohistochemical staining, and are hence time consuming and relatively labor intensive. Second harmonic generation detection using MPM has been used to examine several dermatological conditions including studies observing melanin distribution [1]. The major strength of the SHG detection method is that no immunohistochemical staining is required; therefore long-term monitoring can be performed on the same tissue area without the possibility of image degradation or the need to take skin biopsies. This study demonstrates the feasibility of MPM application to detect collagen SHG in human, porcine and ovine burn tissues, for comparison with normal or control skin.

To verify that the SHG signal detected using MPM was collagen, colocalization of SHG and collagen I by immunohistochemical staining was performed. Although the two signals have similar patterns, the signals did not entirely overlap. One explanation is that a large proportion of the SHG signal detected was collagen III instead of or as well as collagen I. In normal human skin, the collagen I to collagen III ratio is about 3:1, however after burn, the ratio can dramatically alter to 2:1 [25]. After the gradual process of tissue remodeling, collagen III gets replaced by collagen I. Cuttle et al. [26] has described a method for detecting different collagen subtypes in burn tissues using Sirius red staining and polarization microscopy. Thicker and more closely packed collagen fibers such as collagen I exhibited an intense yellow or red birefringence, while relatively thin and looser-packed fibrils such as collagen III often showed a weaker, green tinged birefringence [27]. Although the SHG detection method cannot differentiate between different collagen subtypes, this non-invasive technique still benefits dermatological studies as there are no concerns about sample bleaching. Unfortunately, both the Sirius red method and the SHG collagen detection methods are dependent on collagen fiber density. Newly forming collagen I may be incorrectly identified as collagen III using the Sirius red method, and weak signals from thin fibrils could similarly be missed using the SHG detection method. The observation of mature scars would be expected to exhibit less variability using the SHG detection method, as examination of total collagen architecture is more important than being able to

differentiate between different collagen types, and collagen fibers in mature scar would be of sufficient thickness to allow for sufficiently sensitive SHG detection. One advantage of SHG is in examining total global collagen fiber arrangement and architecture rather than detecting collagen subtypes.

Various studies recently published have used excitation wavelengths from 800 nm to 860 nm with an emission wavelength from 393 nm to 436 nm [17,18,24,28]. Our results show that the best SHG signal is detected at an excitation wavelength of 860 nm using the emissions filter that collects laser signals from 390 nm to 465 nm regardless of the tissue processing technique or species tissue origin. Previously, Chen et al. [18] have described the detection of SHG in human hypertrophic scars using 3-dimensional modeling and Z-stacking methods, and have shown that collagen SHG signal intensity in normal tissue was roughly 1.5 times that in the hypertrophic scar tissue. In Fig. 2, our data did not demonstrate any difference in SHG signal intensity between normal and hypertrophic scar tissues in human samples. This could be due to the difference in sample age such that collagen fibers in children less than one year of age may be thinner and arranged in a different manner compared to teenagers/adolescents. However, it is very difficult to obtain age-, sex-, ethnic background- and body site-matched control human dermal tissue and foreskin tissue was our best option to use as a control in this study.

In this study, although our tissue samples were only 5  $\mu$ m thick, we demonstrated similar collagen architecture described by Linares et al. [12] and Chen et al. [18] and this was confirmed by subsequent collagen fiber observations using hematoxylin and eosin (H&E) stained tissue in identical samples examined by SHG. Normal dermal architecture shows randomly oriented collagen fibers, while hypertrophic scars show elongated collagen bundles of undulating fibers. No obvious collagen nodules were detected in the hypertrophic scar tissues, possibly due to the relatively young age of the scars and the different body sites, and therefore differences in amounts of collagen cross-linkage and packing. Furthermore, there was a greater frequency of collagen with a more nested arrangement in human Scar sample 2 compared to human Scar sample 1. Again, this may be due to a slightly greater maturation of Scar 2 leading to changes in scar morphology or the different body sites that the scars were formed.

Among the various animal models used in skin wound and particularly burns research, the pig burn model is the most similar to human burn wounds in terms of skin structure, scale, composition, physiology and reaction to injury [29-33]. As shown in Fig. 2, the collagen architecture in porcine skin tissue was similar to that in human tissue, although each of the basket-weave collagen arrangements in normal porcine skin were more widely spaced compared to control human skin, which could be due to the differences in body size or site. Similar but less high resolution changes in collagen bundles were also detected in H&E stained sections in all species examined. Our results therefore provide further evidence that the porcine model is suitable for SHG collagen analysis. Although the ovine model is often used in fetal studies, the lack of species-specific antibodies can limit research using these animals as models. Our results demonstrated that SHG detection using MPM was a quick and powerful method to

study collagen in the ovine model. It was sensitive enough to identify thin collagen fibers in ovine fetal dermal tissue and thin or newly formed collagen fibers after burn as well as the morphological changes occurring in thick, deep dermal collagen bundles. Our success in detecting SHG in porcine and ovine dermal tissues shows the potential of applying this method to study collagen deposition in various diseases and animal models. Other researchers have validated the use of SHG detection in mouse skin and after lung fibrosis [16,34], further demonstrating the potential of SHG detection in dermatological research and research into dermal scarring.

This study demonstrated that high resolution collagen architecture in human, porcine and ovine tissue samples can be detected using SHG and MPM without the need for immunofluorescent staining on frozen tissue or paraffin-embedded tissue sections. Although embedding artifacts present in cryostat and paraffin-embedded sections can still be seen to a lesser extent, tissue architecture using the paraffin-embedded method is better preserved and the samples can be kept for longer periods with only simple storage requirements. Our study highlights the future potential for *in vivo* three-dimensional SHG monitoring of clinical patients to examine collagen architecture from an early stage after injury to identify any early pathogenic signs of hypertrophic scar formation. However, while the benefit and usefulness of *in vivo* application of MPM collagen assessment is theoretically possible, there still remain several issues affecting its usefulness for imaging in living animals. These include the ability of keeping the animals from moving to allow adequate image collection, and secondly the limitations in penetration of MPM microscopy to visualize deep into scar tissue. This method is highly sensitive to movements such as respiratory or involuntary nervous reflex movements, and the imaging depth of MPM in skin is only limited to about 200  $\mu\text{m}$ . Therefore, to allow this method to work in live animal or clinical patients, scanning rates and imaging depth will have to be significantly improved through better the microscope design. Other than its clinical use, this approach also benefits dermatological research that involves animal models or human patients when species-specific antibodies are unavailable and painful biopsies have been refused. It can be an efficient technique clinically, as well as for histologically preserved tissue samples. Future studies should be carried out using this approach to examine a larger sample size of pathogenic scars compared to control tissue, to identify the key differences in collagen fiber organization and potentially the complex pathomechanisms of hypertrophic scarring.

### Conflict of interest

The authors have no conflict of interest.

### Acknowledgements

We would like to thank all the participants involved in this study. This work was funded by the Royal Children's Hospital Foundation and a New Staff Start Up Grant from The University of Queensland and by a grant-in-aid to J.R.M. from

the Health and Labor Sciences Research Grant (research into specific diseases) H17-Saisei-12 to Hokkaido University (Japan). A.C.-H.C. is a recipient of The University of Queensland Australian Postgraduate Award scholarship. The fibronectin hybridoma supernatant HFN7.1 developed/donated by R.J. Klebe was obtained from the Developmental Studies Hybridoma Bank, developed under the auspices of the National Institute of Child Health and Development (NICHD) and maintained by the University of Iowa, Department of Biological Sciences, Iowa City, IA 52242, United States.

### REFERENCES

- [1] König K, Riemann I. High-resolution multiphoton tomography of human skin with subcellular spatial resolution and picosecond time resolution. *J Biomed Opt* 2003;8(July (3)):432-9.
- [2] Freund I, Deutsch M, Sprecher A. Connective tissue polarity. Optical second-harmonic microscopy, crossed-beam summation, and small-angle scattering in rat-tail tendon. *Biophys J* 1986;50(October (4)):693-712.
- [3] Kim BM, Eichler J, Da Silva LB. Frequency doubling of ultrashort laser pulses in biological tissues. *Appl Opt* 1999;38(December (34)):7145-50.
- [4] Kim BM, Eichler J, Reiser KM, Rubenchik AM, Da Silva LB. Collagen structure and nonlinear susceptibility: effects of heat, glycation, and enzymatic cleavage on second harmonic signal intensity. *Lasers Surg Med* 2000;27(4):329-35.
- [5] Campagnola PJ, Millard AC, Terasaki M, Hoppe PE, Malone CJ, Mohler WA. Three-dimensional high-resolution second-harmonic generation imaging of endogenous structural proteins in biological tissues. *Biophys J* 2002;82(January (1 Pt 1)):493-508.
- [6] Roediger B, Ng LG, Smith AL, de St Groth BF, Weninger W. Visualizing dendritic cell migration within the skin. *Histochem Cell Biol* 2008;130(December (6)):1131-46.
- [7] Schenke-Layland K, Riemann I, Damour O, Stock UA, König K. Two-photon microscopes and *in vivo* multiphoton tomographs—powerful diagnostic tools for tissue engineering and drug delivery. *Adv Drug Deliv Rev* 2006;58(September (7)):878-96.
- [8] König K, Ehlers A, Stracke F, Riemann I. *In vivo* drug screening in human skin using femtosecond laser multiphoton tomography. *Skin Pharmacol Physiol* 2006;19(2):78-88.
- [9] Raffetto JD, Khalil RA. Matrix metalloproteinases in venous tissue remodeling and varicose vein formation. *Curr Vasc Pharmacol* 2008;6(July (3)):158-72.
- [10] Schwanholt CA, Ridgway CL, Greenhalgh DG, Staley MJ, Gaboury TJ, Morress CS, et al. A prospective study of burn scar maturation in pediatrics: does age matter? *J Burn Care Rehabil* 1994;15(September-October (5)):416-20.
- [11] Rochet JM, Zaoui A. Burn scars: rehabilitation and skin care. *Rev Prat* 2002;52(December (20)):2258-63.
- [12] Linares HA, Kischer CW, Larson DL, Dobrkovs M. Histotypic organization of hypertrophic scar in humans. *J Invest Dermatol* 1972;59(October (4)):323-31.
- [13] Cuttle L, Kempf M, Phillips GE, Mill J, Hayes MT, Fraser JF, et al. A porcine deep dermal partial thickness burn model with hypertrophic scarring. *Burns* 2006;32(7):806-20.
- [14] Fraser JF, Cuttle L, Kempf M, Phillips GE, O'Rourke PK, Choo K, et al. Deep dermal burn injury results in scarless wound healing in the ovine fetus. *Wound Repair Regen* 2005;13(March-April (2)):189-97.



- [15] Yeh AT, Kao BS, Jung WG, Chen ZP, Nelson JS, Tromberg BJ. Imaging wound healing using optical coherence tomography and multiphoton microscopy in an in vitro skin-equivalent tissue model. *J Biomed Opt* 2004;9(March-April (2)):248-53 [article].
- [16] Pena AM, Fabre A, Debarre D, Marchal-Somme J, Crestani B, Martin JL, et al. Three-dimensional investigation and scoring of extracellular matrix remodeling during lungfibrosis using multiphoton microscopy. *Microsc Res Tech* 2007;70(February (2)):162-70 [article].
- [17] Da Costa V, Wei R, Lim R, Sun CH, Brown JJ, Wong BJF. Nondestructive imaging of live human keloid and facial tissue using multiphoton microscopy. *Arch Facial Plast Surg* 2008;10(January-February (1)):38-43 [article].
- [18] Chen G, Chen J, Zhuo S, Xiong S, Zeng H, Jiang X, et al. Nonlinear spectral imaging of human hypertrophic scar based on two-photon excited fluorescence and second-harmonic generation. *Br J Dermatol* 2009;161(July (1)):48-55 [article].
- [19] Bancroft JD, Stevens A. *Theory and practice of histological techniques*. Churchill Livingstone: London; 1996.
- [20] Kidd KR, Williams SK. Laminin-5-enriched extracellular matrix accelerates angiogenesis and neovascularization in association with ePTFE. *J Biomed Mater Res A* 2004;69(May (2)):294-304.
- [21] Schoen RC, Bentley KL, Klebe RJ. Monoclonal antibody against human fibronectin which inhibits cell attachment. *Hybridoma* 1982;1(2):99-108.
- [22] McMillan JR, McGrath JA, Pulkkinen L, Kon A, Burgeson RE, Ortonne JP, et al. Immunohistochemical analysis of the skin in junctional epidermolysis bullosa using laminin 5 chain specific antibodies is of limited value in predicting the underlying gene mutation. *Br J Dermatol* 1997;136(June (6)):817-22.
- [23] Wrenn DS, Griffin GL, Senior RM, Mecham RP. Characterization of biologically active domains on elastin: identification of a monoclonal antibody to a cell recognition site. *Biochemistry* 1986;25(September (18)):5172-6.
- [24] Lu KC, Chen JX, Zhuo SM, Zheng LQ, Jiang XS, Zhu XQ, et al. Multiphoton laser scanning microscopy of localized scleroderma. *Skin Res Technol* 2009;15(November (4)):489-95 [article].
- [25] Prockop DJ, Kivirikko KI, Tuderman L, Guzman NA. Biosynthesis of collagen and its disorders, 1. *N Engl J Med* 1979;301(1):13-23 [review].
- [26] Cuttle L, Nataatmadja M, Fraser JF, Kempf M, Kimble RM, Hayes MT. Collagen in the scarless fetal skin wound: detection with picrosirius-polarization. *Wound Repair Regen* 2005;13(March-April (2)):198-204.
- [27] Montes GS, Junqueira LC. The use of the Picrosirius-polarization method for the study of the biopathology of collagen. *Mem Inst Oswaldo Cruz* 1991;86(Suppl. 3):1-11.
- [28] Chen JX, Lee A, Zhao JH, Wang HQ, Lui H, McLean DI, et al. Spectroscopic characterization and microscopic imaging of extracted and in situ cutaneous collagen and elastic tissue components under two-photon excitation. *Skin Res Technol* 2009;15(November (4)):418-26 [article].
- [29] Montagna W, Yun JS. The skin of the domestic pig. *J Invest Dermatol* 1964;42(July):11-21.
- [30] Wang XQ, Liu PY, Kempf M, Cuttle L, Chang AH, Wong M, et al. Burn healing is dependent on burn site: a quantitative analysis from a porcine burn model. *Burns* 2009;35(March (2)):264-9.
- [31] Wang XQ, Kravchuk O, Liu PY, Kempf M, Boogaard CV, Lau P, et al. The evaluation of a clinical scar scale for porcine burn scars. *Burns* 2009;35(June (4)):538-46.
- [32] Meyer W, Schwarz R, Neurand K. The skin of domestic mammals as a model for the human skin, with special reference to the domestic pig. *Curr Probl Dermatol* 1978;7:39-52.
- [33] Sullivan TP, Eaglstein WH, Davis SC, Mertz P. The pig as a model for human wound healing. *Wound Repair Regen* 2001;9(March-April (2)):66-76.
- [34] Luo T, Chen JX, Zhuo SM, Lu KC, Jiang XS, Liu QG. Visualization of collagen regeneration in mouse dorsal skin using second harmonic generation microscopy. *Laser Phys* 2009;19(March (3)):478-82 [article].

# Topical Cholecystokinin Depresses Itch-Associated Scratching Behavior in Mice

Shoko Fukamachi<sup>1</sup>, Tomoko Mori<sup>1</sup>, Jun-Ichi Sakabe<sup>1</sup>, Noriko Shiraishi<sup>1</sup>, Etsushi Kuroda<sup>2</sup>, Miwa Kobayashi<sup>1</sup>, Toshinori Bito<sup>3</sup>, Kenji Kabashima<sup>4</sup>, Motonobu Nakamura<sup>1</sup> and Yoshiki Tokura<sup>1,5</sup>

Cholecystokinin (CCK) serves as a gastrointestinal hormone and also functions as a neuropeptide in the central nervous system (CNS). CCK may be a downregulator in the CNS, as represented by its anti-opioid properties. The existence of CCK in the peripheral nervous system has also been reported. We investigated the suppressive effects of various CCKs on peripheral pruritus in mice. The clipped backs of ICR mice were painted with CCK synthetic peptides and injected intradermally with substance P (SP). The frequency of SP-induced scratching was reduced significantly by topical application of sulfated CCK8 (CCK8S) and CCK7 (CCK7S), but not by nonsulfated CCK8, CCK7, or CCK6. Dermal injection of CCK8S also suppressed the scratching frequency, suggesting that dermal cells as well as epidermal keratinocytes (KCs) are the targets of CCKs. As determined using real-time PCR, mRNA for CCK2R, one of the two types of CCK receptors, was expressed highly in mouse fetal skin-derived mast cells (FSMCs) and moderately in ICR mouse KCs. CCK8S decreased *in vitro* compound 48/80-promoted degranulation of FSMCs with a transient elevation of the intracellular calcium concentration. These findings suggest that CCK may exert an antipruritic effect via mast cells and that topical CCK may be clinically useful for pruritic skin disorders.

*Journal of Investigative Dermatology* (2011) 131, 956–961; doi:10.1038/jid.2010.413; published online 3 February 2011

## INTRODUCTION

Itch or pruritus is an unpleasant cutaneous sensation associated with the immediate desire to scratch (Ikoma *et al.*, 2006; Steinhoff *et al.*, 2006). Histamine was long considered the only mediator of pruritus, but this assumption has changed dramatically in the past two decades. Peripheral itch can be evoked in the skin either directly, by mechanical and thermal stimuli, or indirectly, through chemical mediators (Ikoma *et al.*, 2006). Itch may also be generated in the central nervous system (CNS) independent of peripheral stimulation. Different pruritic diseases involved different itch mediators, including histamine, neuropeptides, proteases, prostaglandins, serotonin, acetylcholine, cannabinoids, opioids, bradykinins, cytokines, biogenic amines, neurotransmitters, and ion channels (Steinhoff *et al.*, 2006).

Neuromediators such as neuropeptides and neurotrophins, as well as their receptors, have an important role in peripheral itch. Neuropeptides, as represented by pruritogenic neuropeptide substance P (SP), are produced by sensory nerves, but they can also be elaborated by epidermal keratinocytes (KCs), mast cells, fibroblasts, and other cutaneous immunocompetent cells (Ohkubo and Nakanishi, 1991; Scholzen *et al.*, 1998). Many other mediators are also produced by and secreted from skin-constituent cells in close contact to sensory nerves (Steinhoff *et al.*, 2006). They can activate and sensitize pruritic nerve endings and even modulate their growth, as do nerve growth factors and chemorepellents (Yamaguchi *et al.*, 2008; Yosipovitch and Papoiu, 2008). As for the receptor system, it is notable that KCs, mast cells, and fibroblasts express neurokinin-1 receptor (Ohkubo and Nakanishi, 1991; Scholzen *et al.*, 1998), which is the receptor for SP. These complicated neurophysiological interactions yield itch and render its therapeutic control difficult.

Cholecystokinin (CCK) is a peptide hormone in the gastrointestinal tract (Dufresne *et al.*, 2006), but it also serves as a neuropeptide (Ma *et al.*, 2006). Among neuropeptides, CCKs are most abundantly present in the CNS and involved in numerous physiological functions such as anxiety, depression, psychosis, memory, and feeding behavior (Dufresne *et al.*, 2006). CCKs also have anti-opioid properties in the CNS (Pommier *et al.*, 2002; Mollereau *et al.*, 2005) and exert a nociceptive effect in the spinal cord (Wiesenfeld-Hallin *et al.*, 1999). Furthermore, their existence in the peripheral nervous system has been reported (Moriarty *et al.*, 1997). In various CCKs, sulfation of the tyrosine at position 7

<sup>1</sup>Department of Dermatology, University of Occupational and Environmental Health, Kitakyushu, Japan; <sup>2</sup>Department of Immunology, University of Occupational and Environmental Health, Kitakyushu, Japan; <sup>3</sup>Department of Dermatology, Kobe University, Kobe, Japan; <sup>4</sup>Department of Dermatology, Kyoto University Graduate School of Medicine, Kyoto, Japan and <sup>5</sup>Department of Dermatology, Hamamatsu University School of Medicine, Hamamatsu, Japan

Correspondence: Yoshiki Tokura, Department of Dermatology, Hamamatsu University School of Medicine, 1-20-1 Handayama, Higashi-Ku, Hamamatsu 431-3192, Japan. E-mail: tokura@hama-med.ac.jp

Abbreviations: CCK, cholecystokinin; CCK2R, CCK2 receptor; CCK7S, sulfated CCK7; CCK8S, sulfated CCK8; CNS, central nervous system; FSMC, murine fetal skin-derived mast cell; KC, keratinocyte; SP, substance P

Received 15 February 2010; revised 3 November 2010; accepted 12 November 2010; published online 3 February 2011

from the C-terminus is a posttranslational modification that makes them biologically active peptides (Ma *et al.*, 2006). Varying lengths of CCKs with or without sulfate have been studied for their activities as gastrointestinal hormones (Bonetto *et al.*, 1999) and as CNS players (Rehfeld *et al.*, 2007). Two types of CCK receptors have been identified: CCK1R (CCK-A receptor) and CCK2R (CCK-B receptor). CCK1R usually requires sulfated CCKs. CCK2R affords a binding site to both sulfated and nonsulfated ligands, but nonsulfated CCKs have affinities that are decreased 10- to 50-fold (Dufresne *et al.*, 2006). CCKs exert their biological functions by interacting with CCK receptors located on multiple target cells in the CNS and on peripheral nerve endings (Dufresne *et al.*, 2006; Rehfeld *et al.*, 2007; Zheng *et al.*, 2009). In the brain, sulfated CCK8 (CCK8S) is most abundant (Rehfeld *et al.*, 2007) and possesses one of the strongest endogenous anti-opioid properties (Ma *et al.*, 2006). Prolonged opioid exposure increases the expression of CCKs and CCK2R in the CNS, where CCK8S negatively modulates opioid responses and maintains homeostasis of the opioid system (Pommier *et al.*, 2002; Agnes *et al.*, 2008). Thus, it seems that CCKs are downregulators of opioid-mediated pruritus in CNS. However, the function of CCKs, the distribution of CCK receptors in the skin, and their effects on peripheral pruritus remain unelucidated (Ma *et al.*, 2006).

In this study, we investigated the antipruritic effects of different lengths of CCKs with or without sulfate, which were topically applied onto the skin of mice. Results suggest that CCKs are capable of reducing SP-induced scratching at least by affecting the function of mast cells. Our findings may lead to the development of previously unreported antipruritic strategies.

## RESULTS

### Depressive effects of topical application of CCKs on SP-induced itch-associated response

We tested various CCKs for their ability to suppress scratching behavior induced by intradermal SP injection in ICR mice (Andoh *et al.*, 2001). We first examined the effect of percutaneously applied CCK on the response. Because CCK8S has an inhibitory ability in the CNS (Pommier *et al.*, 2002; Dufresne *et al.*, 2006) and gastrointestinal tract (Miyasaka *et al.*, 2004), CCK8S and the other CCK constructs consisting of smaller amino acids with or without sulfate (Table 1) were tested for their antipruritic activities. ICR mice were painted with various CCKs on the clipped, tape-stripped rostral part of the back skin (~1.8 cm<sup>2</sup>) and then injected with SP intradermally at the CCK-painted site.

The topical application of CCK8S significantly reduced the scratching frequency, as compared with the nonapplied control (Figure 1a), whereas nonsulfated CCK8, CCK7, and CCK6 had no ability to suppress scratching. These results showed that CCKs have an antipruritic ability, and CCK constructs bearing sulfation of position 7 are required for the ability to suppress the scratching behavior. In this itch-associated-scratching model, we also administered CCK8S intradermally together

**Table 1. Amino acid sequences of CCK and its constructs**

Sulfated CCK8 (CCK8S)	Asp-Tyr (SO <sub>3</sub> <sup>-</sup> )-Met-Gly-Trp-Met-Asp-Phe-NH <sub>2</sub>
Nonsulfated CCK8 (CCK8)	Asp-Tyr-Met-Gly-Trp-Met-Asp-Phe-NH <sub>2</sub>
Sulfated CCK7 (CCK7S)	Tyr (SO <sub>3</sub> <sup>-</sup> )-Met-Gly-Trp-Met-Asp-Phe-NH <sub>2</sub>
Nonsulfated CCK7 (CCK7)	Tyr-Met-Gly-Trp-Met-Asp-Phe-NH <sub>2</sub>
Nonsulfated CCK6 (CCK6)	Met-Gly-Trp-Met-Asp-Phe-NH <sub>2</sub>

Abbreviation: CCK, cholecystokinin.

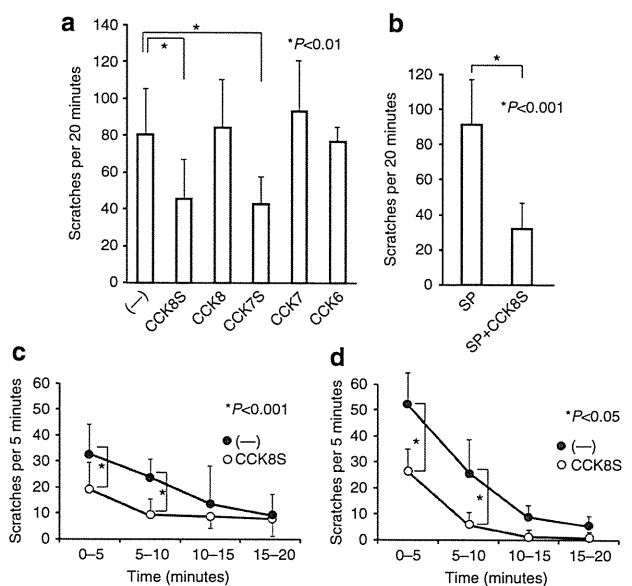


**Figure 1. Suppression of substance P (SP)-induced itch by percutaneous application or intradermal injection of cholecystokinins (CCKs).** (a) ICR mice were painted on the clipped skin with CCKs (0.5 nmol per site) and injected intradermally with SP (100 nmol per site). The group depicted with “(-)” represents mice injected with vehicle (acetone/olive oil) alone. The numbers of mice were as follows: CCK (-), *n* = 12; CCK8S, *n* = 10; CCK8, *n* = 6; CCK7S, *n* = 6; CCK7, *n* = 3; and CCK6, *n* = 4. (b) ICR mice were injected intradermally with SP or with SP and CCK8S. Each bar represents the mean of scratches per 20 minutes. CCK (-), *n* = 5 and CCK8S, *n* = 8. (c) Time course of scratching frequency in mice untreated (*n* = 12) or topically administered CCK8S (*n* = 10). (d) Time course of scratching frequency in mice untreated (*n* = 5) or intradermally injected with CCK8S (*n* = 8). CCK7, nonsulfated CCK7; CCK8, nonsulfated CCK8; CCK7S, sulfated CCK7; CCK8S, sulfated CCK8.

with SP to mice. The scratching frequency induced by SP was profoundly suppressed by the simultaneous injection of CCK8S (Figure 1b). When the time course of effects induced by CCK8S was examined, both topical application (Figure 1c) and intradermal injection (Figure 1d) of CCKs reduced the scratching frequency at intervals of 0–5 minutes and 5–10 minutes.

These findings raised the possibility that epidermal and dermal cells participating in the development of itch are affected by CCKs.

### CCK2R expression in KCs and mast cells

Both KCs and mast cells are the possible targets of CCKs in the suppression of SP-induced pruritus. It is known that KCs express the receptors for itch-related molecules, neurokinin-1 receptor for SP, H1 receptor for histamine, and protease-activated receptor-2 for tryptase (synthetic agonist, SLIGRL-NH<sub>2</sub>). Mast cells are well known to possess neurokinin-1 receptor (Scholzen *et al.*, 1998; Liu *et al.*, 2006). We investigated the expression of the CCK receptors CCK1R and CCK2R in KCs and mast cells. Primary cultures of KCs from ICR mice and fetal skin-derived mast cells (FSMCs) were collected, and mRNAs for CCK1R and CCK2R were quantitated by real-time PCR, RT-PCR, and western blotting analyses. The two types of cells expressed both CCK1R and CCK2R at the mRNA and protein levels (Figure 2). When the expression levels of real-time PCR analysis were normalized with the  $\beta$ -actin

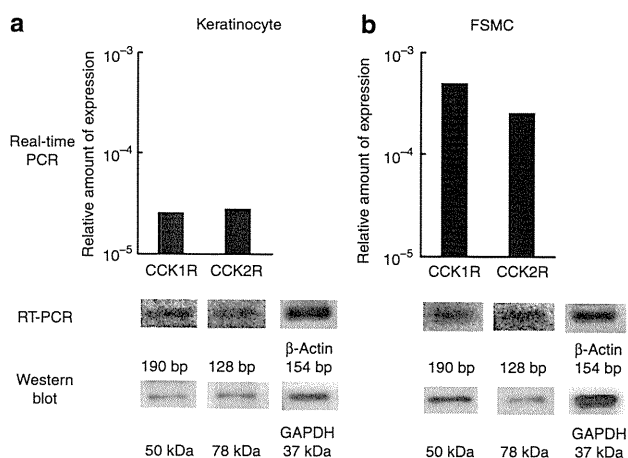


**Figure 2. CCK-A receptor (CCK1R) and CCK-B receptor (CCK2R) mRNA expression in keratinocytes and mast cells.** Cultured ICR mouse keratinocytes (a) and fetal skin-derived mast cells (FSMCs) (b) were examined for the expression of mRNAs for CCK1R and CCK2R using real-time PCR and RT-PCR and for the expression of their proteins using western blotting analysis. Data are expressed as the amount of expression relative to  $\beta$ -actin. Glyceraldehyde-3-phosphate dehydrogenase (GAPDH) was used as control for western blotting.

level, the two receptors were more highly expressed in FSMCs than in KCs.

In a preliminary DNA microarray analysis of normal human epidermal KCs, we investigated the levels of gene expression from stimulation with SP ( $10^{-6}$  M), histamine ( $10 \mu\text{g ml}^{-1}$ ), or SLIGRL-NH<sub>2</sub> (100 nM) under high calcium (0.6 mM) concentration. The CCK2R expression by SP-stimulated KCs was most elevated; its level was  $2^{8.67}$  times that of the control (Supplement Data online). Such an increased CCK2R expression was not observed with histamine or SLIGRL-NH<sub>2</sub>. This observation suggested that CCK2R has an important role in the suppression of SP-stimulated KCs. To determine the effect of SP on KCs, ICR mouse KCs were incubated with SP for 30 minutes to 24 hours, and the expression of CCK2R and CCK1R was analyzed by western blotting. CCK2R was detected with antibodies as a 78 kDa band (Morisset *et al.*, 2003) and increased in KCs exposed to SP for 5 or 6 hours (Figure 3a). By contrast, CCK1R expression was not augmented by SP (Figure 3b). Thus, the expression of some receptors for CCK is enhanced by SP, depending on the receptor.

### Suppression of FSMC degranulation by CCK8S with transient elevation of intracellular calcium

The above findings suggested that CCKs bind to CCK2R on KCs and mast cells and downmodulate their itch-related biological functions. Given that the level of CCK2R expression was higher in FSMCs than in KCs and the application of CCKs immediately exerted its inhibitory effects on the scratching behavior, it is possible that CCKs directly affect mast cells. We therefore focused on mast cells as the primary target. The addition of compound 48/80 induced degranulation of FSMCs (Figure 4a). This promoted degranulation of FSMCs, which was significantly inhibited by CCK8S at  $10^{-8}$  or  $10^{-7}$  M concentration.

To test whether CCK8S evokes signal transduction in mast cells, we measured the intracellular calcium using confocal recording. The fluorescence intensity of 15 cells positively responding on addition of CCK8S was monitored with computerized color change on a display using a digital image processing system. The mast cells exhibiting green fluorescence of Fluo-4-AM at any time point between 40 and

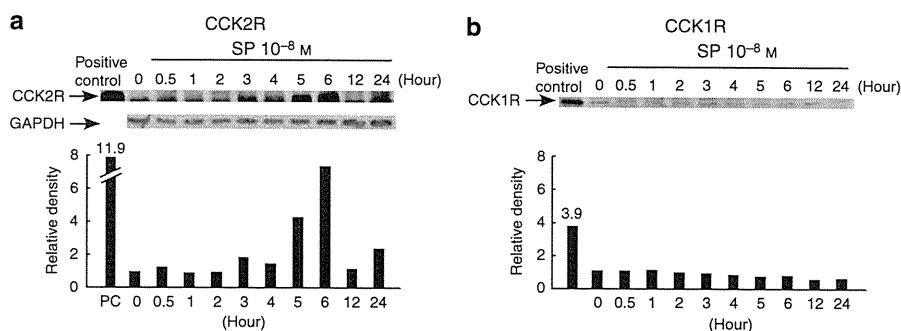


**Figure 3. Western blotting of CCK-A receptor (CCK1R) and CCK-B receptor (CCK2R) in mouse keratinocytes stimulated with substance P (SP).** ICR mouse keratinocytes were incubated with SP ( $10^{-8}$  M) for 0.5–24 hours and harvested at each time point. The expression levels of CCK2R (a) and CCK1R (b) were analyzed by western blotting. NIH/3T3 whole lysates were used as positive control. Glyceraldehyde-3-phosphate dehydrogenase (GAPDH) was used as control for western blotting and exhibited similar intensities in the samples cultured for 0–24 hours. The intensity of each band was subjected to densitometric analysis and expressed as density relative to the nontreated control (0).

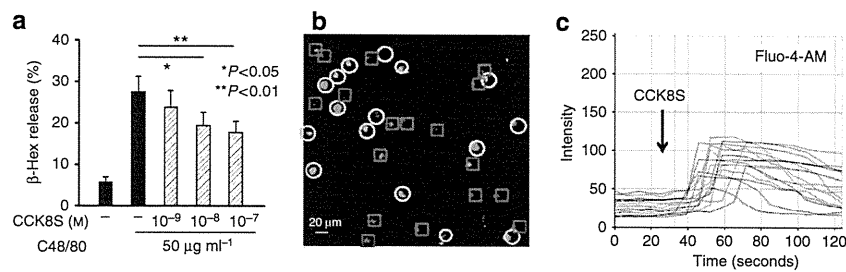


**Figure 4. Suppression of fetal skin-derived mast cell (FSMC) degranulation by sulfated CCK8 (CCK8S) with transient intracellular calcium increase.** (a) FSMCs were incubated with or without CCK8S in the presence of compound 48/80 (C48/80; 50 µg ml<sup>-1</sup>) for 15 minutes. Supernatants and cell lysates were incubated with *p*-nitrophenyl-*N*-acetyl-β-D-galactosaminide, and β-hexosaminidase (β-Hex) release was determined as the ratio between activity in the supernatant and cell lysate, multiplied by 100. (b) FSMCs were loaded with Fluo-4-AM (green) and stained for CD117 (c-kit, red). The percentage of CCK8S-responding FSMCs was determined from the fluorescence traces of all cells. Circles represent responding FSMCs and squares represent nonresponding FSMCs. Bar = 20 µm. (c) The addition of CCK8S to FSMC culture induced an increase in intracellular calcium level.

80 seconds after CCK8S addition were defined as positively responding cells (Figure 4b and c); these are marked with a yellow circle in Figure 4b. The addition of CCK8S to the FSMC culture induced a prompt rise of calcium that persisted for more than 2 minutes and then gradually declined, indicating that CCK8S induces signaling via CCK2R in mast cells. The percentage of responding FSMCs was determined from the fluorescence traces of all cells. As shown in Figure 4b, in which circles and squares represent CCK8S-responding and nonresponding FSMCs, respectively, 45% (16 of 36 cells) of FSMCs were typically activated by CCK8S.

## DISCUSSION

Despite their original name of cholecyst stimulators, CCKs have been known to serve as CNS modulators (Dufresne *et al.*, 2006) and CCK8S downmodulates opioid responses (Pommier *et al.*, 2002; Agnes *et al.*, 2008). As suggested in our present study, CCKs may also have a function of downmodulator in the peripheral itch. The topical application of CCKs suppressed the itch-related scratching behavior evoked by SP injection. The expression of CCK2R, but not CCK1R, in murine and human KCs was markedly enhanced by exposure to SP. It is likely that CCK2R, whose expression is augmented by SP, has a down-regulatory role in the excess peripheral itch.

Among the CCK constructs consisting of different numbers of amino acids with or without sulfate, CCK8S and CCK7S, but not CCK8, CCK7, or CCK6, exerted an antipruritic action. Therefore, in a comparison between CCK8S and CCK8 and between CCK7S and CCK7, sulfation of position 7 is required for the ability to suppress the scratching behavior. This is in accordance with the observation that CCK8S has an anxiogenic effect (Harro, 2006), a depressant effect, and an anti-opioid effect (Noble *et al.*, 1999), but the effects of CCK are limited by desulfation of the tyrosine (Tokunaga *et al.*, 1993).

Although the exact mode of antipruritic action of CCKs is still speculative, some informative observations were obtained from the study. Both percutaneous application and dermal injection were effective routes for CCK8S in suppressing itch, suggesting that epidermal and/or dermal constituents are the targets of CCKs. Furthermore, the administration of CCK8S rapidly inhibited the SP-induced itch. We thus investigated the mechanism of CCK suppression of itch in

*in vitro* studies, focusing on mast cells. CCK8S significantly reduced the degranulation of FSMCs with elevation of intracellular calcium concentration, suggesting that mast cell degranulation is inhibited by CCK8S through CCK2R. Alternatively, or additionally, KCs are possibly involved in CCR action. KCs are thought to mediate pruritus by releasing inflammatory mediators and neurotrophins. Therefore, the antipruritic effect of CCK8S on KCs, if any, seems to need a time lag to operate. As the therapeutic action of topical CCK8S is rapid, mast cells may be more likely targeted by CCK8S than KCs. The high expression of CCK2R in mast cells further supports the notion that mast cells are sensitive to CCKs. However, SP was reported to cause scratching behavior in both mast cell-deficient and wild-type mice (Hossen *et al.*, 2003), suggesting a mast cell-independent mechanism of SP-evoked itch. Given this observation, it is possible that another skin constituent, such as the sensory nerves, is affected by CCKs. The target cells and the actions of CCK8S on them warrant elucidation in the future.

The antipruritic effects of CCK8S and CCK7S on this mouse itch model may afford a therapeutic use for the CCKs for the treatment of skin diseases with peripheral itch. Given that the major target of CCKs is mast cells, urticaria, atopic dermatitis, contact dermatitis, and other types of eczematous dermatitis would be successfully treated with CCKs topically applied to the skin. The therapeutic effects of CCKs on peripheral itch may shed light on the mechanisms underlying the physiological regulation of itch, and it is notable that CCKs have potential as a topical drug for pruritic skin diseases.

## MATERIALS AND METHODS

### Animals

Female ICR mice were obtained from KBT Oriental (Tosu, Japan). These mice were maintained in the Laboratory Animal Research Center of the University of Occupational and Environmental Health under specific-pathogen-free conditions and used at the age of 6–8 weeks. All animal experiments were performed according to the guidelines approved by our university for the care and use of animals.

### Reagents

SP, CCK8S, nonsulfated CCK8, CCK7S, and nonsulfated CCK6 were purchased from the Peptide Institute (Osaka, Japan). Nonsulfated

CCK7 was purchased from Funakoshi (Tokyo, Japan). Compound 48/80 was purchased from Sigma (St Louis, MO).

### Itch-associated scratching behavior and topical application of CCKs

The hair was clipped over the rostral part of the each mouse's back 1 or 2 days before the experiment. Before behavioral recording, each animal (four per observation) was put into an acrylic cage (18 × 23 × 11 cm) for at least 1 hour for acclimation. An intradermal injection of SP (100 nmol in 50 μl of physiological saline per site) induced scratching of the skin around the injected site with the hindpaws (Andoh *et al.*, 2001). CCKs were topically applied in two ways: percutaneous application and intradermal injection. For percutaneous application, the shaved back skin was stripped with Scotch tape (3M) six times on the day before the experiment (Nishijima *et al.*, 1997). The clipped backs of the mice were painted (1.8 cm<sup>2</sup>, 1.5 cm in diameter) with 20 μl CCK (0.5 nmol per site) in acetone/olive oil (3:1) 3–4 minutes before the SP injection (100 nmol per site). For intradermal application, mice were injected intradermally with CCK (0.5 nmol per site in 20 μl physiological saline), followed immediately by SP injection at the same site (100 nmol per site). Immediately after treatment, the animals were put back into the same cage and their behavior was videotaped for 40 minutes using a digital video camera (Andoh *et al.*, 2001). Using the video, the frequency of scratching toward the injected site by the hindpaws was recorded for the first 20 minutes.

### Murine KCs

The skin of ICR newborn mice was peeled within 24 hours after birth and incubated with 0.05% collagenase (collagenase from *Clostridium histolyticum* type 2; Sigma) for 2 days at 37 °C in a 5% CO<sub>2</sub> atmosphere. Epidermal sheets were collected and suspended in culture medium. Cell suspension was plated into six-well plates (Corning Glass Works, Corning, NJ) and grown to subconfluence in CnT-07 medium (Funakoshi).

### Murine mast cells

The method for preparation of murine FSMCs has been described previously (Yamada *et al.*, 2003). Day 14 fetal skin was dissociated by 0.25% trypsin for 20 minutes at 37 °C in Hank's balanced salt solution (Gibco, Carlsbad, CA). Erythrocytes were lysed using RBC-lysing buffer (Sigma) and, after washing, cells were resuspended in complete RPMI, which is RPMI-1640 (Gibco) supplemented with 5% fetal bovine serum (Gibco), 1% nonessential amino acids (Gibco), 1% sodium pyruvate (Gibco), antibiotic/antimycotic (Invitrogen, Carlsbad, CA), and 0.1% 2-mercaptoethanol (Gibco). Fifty milliliters of the cell suspension in each 175 cm<sup>2</sup> 75-flask (Corning Glass Works) was cultured in the presence of 20 ng ml<sup>-1</sup> recombinant mouse IL-3 (Invitrogen) and 20 ng ml<sup>-1</sup> recombinant mouse stem cell factor (Biosource, Camarillo, CA) at 37 °C without changing the medium. Nonadherent and loosely adherent cells were harvested. The cells were centrifuged and resuspended in RPMI, layered on 40% Percoll (GE Healthcare, Buckinghamshire, England), and centrifuged at room temperature. The cell pellet at the bottom was used as FSMCs. For flowcytometric analysis, cells were stained with phycoerythrin-conjugated anti-mouse FcεRI (eBioscience, San Diego, CA) and Alexa Fluor 700-conjugated anti-mouse CD117 (c-kit; eBioscience) for 20 minutes on ice, washed twice, and then resuspended with FACS

buffer. Flow cytometric analysis was performed with FACS Canto (BD, Franklin Lakes, NJ) and FlowJo software (TreeStar, San Carlos, CA). The purity of FSMCs was 95%, as determined by both FcεRI and CD117 positivity by flow cytometry.

### Real-time quantitative RT-PCR analysis

Total RNA was extracted from the cell pellet using the PureLink RNA Mini Kit (Invitrogen). cDNA was reverse transcribed from total RNA samples using the TaqMan Reverse Transcription reagents (Applied Biosystems, Carlsbad, CA). mRNA expression was quantified by real-time PCR using SYBR Green Dye (PE Biosystems, Foster City, CA) with an ABI PRISM 7000 Sequence Detection System (Applied Biosystems) according to the manufacturer's instructions. Primers were designed using Primer Bank for the human and murine genes, and they were constructed by Invitrogen. The sequences are as follows: murine β-actin: 5'-GGCTGTATCCCTCCATCG-3' and 5'-CCAGTTGGTAAACAATGCCATGT-3'; murine CCK2R: 5'-GATGGCTGCTACGTGCAACT-3' and 5'-CGCACCACCGCTTCTTAG-3'; and murine CCK1R: 5'-CACGCTGGTTATCACGGTG-3' and 5'-GCCATGAAGTAGGTGGTAGTC-3'. The conditions for the real-time PCR were as follows: 2.0 minutes at 50 °C, 10 minutes at 95 °C, and then 50 cycles of amplification consisting of 15 seconds at 95 °C and 1 minute at 60 °C. All heating and cooling steps were performed with a slope of 20 °C per second. Relative expression was calculated using the delta Ct method.

### Western blotting

KCs from ICR mice were stimulated with SP (10<sup>-8</sup> M) in six-well plates (Corning Glass Works) for 0.5–24 hours, harvested with a rubber policeman, and subjected to extraction with RIPA buffer (Wako, Osaka, Japan; 50 mM Tris-HCl (pH8.0), 150 mM sodium chloride, 0.5% (wt/vol) sodium deoxycholate, 0.1% (wt/vol) SDS, and 1.0% (wt/vol) NP-40 substitute). Protein samples (20 μg) were separated by 8% SDS-polyacrylamide gel electrophoresis and electroblotted onto polyvinylidene difluoride membranes for 2 hours at 180 mA. After blocking with 5% skim milk solution, the membranes were incubated with rabbit anti-mouse CCK1R (SC-33220; 1:1,000, Santa Cruz, Santa Cruz, CA), CCK2R (SC-33221; 1:1,000, Santa Cruz), polyclonal antibodies, or GAPDH (SC-25887; 1:1,000, Santa Cruz), and the reaction was detected with horseradish peroxidase-conjugated goat anti-rabbit IgG (1:3,000, Bio-Rad, Hercules, CA). Immunoblots were visualized using the ECL Plus Western Blotting Detection Reagents (GE Healthcare) according to the manufacturer's protocol. Bands were quantified by densitometry with the help of a CS Analyzer version 2.0 (ATTO, Tokyo, Japan). NIH/3T3 whole cell lysate (Santa Cruz) was used as a positive control.

### Mast cell degranulation

Degranulation of FSMCs was assessed by β-hexosaminidase assay (Yamada *et al.*, 2003; Noguchi *et al.*, 2005). FSMCs were washed with Tyrode's buffer (Sigma) and resuspended at a concentration of 2 × 10<sup>4</sup> cells per well into a 96-well plate. FSMCs were incubated with or without CCK8S in the presence of compound 48/80 (50 μg ml<sup>-1</sup>) for 15 minutes at 37 °C. The plate was centrifuged for 5 minutes, and the supernatants were placed into another 96-well plate. Cell pellets were resuspended in Tyrode's buffer containing 0.5% triton X-100 (Sigma). Supernatants and cell lysates (50 μl) were incubated with 100 μl of 2.5 mM *p*-nitrophenyl-*N*-acetyl-β-D-galactosaminide (Sigma),

dissolved in 0.04 mM citrate buffer (pH 4.5), at 37 °C for 90 minutes. The reaction was stopped with 100 µl of 0.4 M glycine (pH 10.7; MP Biomedicals, Solon, OH). The plate was read at 405 nm using a 595 nm reference filter in a microplate reader (Bio-Rad). β-Hexosaminidase release was determined as the ratio between activity in the supernatant and the cell lysate, multiplied by 100.

### Calcium influx determined by confocal imaging

Confocal imaging of cells loaded with fluorescent dyes was performed using a Zeiss LSM5 pascal (Carl Zeiss, Jena, Germany). FSMCs were loaded with Fluo-4-AM (Invitrogen; 1 µM) at 37 °C for 20 minutes, washed twice, and set aside for at least 40 minutes. FSMCs were also stained for CD117 (c-kit) with Alexa Fluor 700-conjugated anti-mouse CD117 antibody. The LSM5 multitrack configuration was used for simultaneous measurement of intracellular calcium concentration (excitation, 488 nm; emission, long-pass 505 nm filter) and the expression of CD117 (excitation, 633 nm; emission, long-pass 650 nm filter). Images were recorded (usually recording for 300 seconds) at room temperature, in a 512 × 512-pixel format. As stimulants, SP or CCKs were added directly to the bath as a small drop (10 µl; final concentration, 10<sup>-6</sup> M SP and 10<sup>-6</sup> M CCK8S). Image data were analyzed offline using the Zeiss LSM510 analyzing software (LSM Image Examiner, Carl Zeiss). The mast cells exhibiting green fluorescence of Fluo-4-AM at any time point between 40 and 80 seconds after CCK8S addition were defined as positively responding cells.

### Gene-array analysis

Normal human epidermal KCs were cultured with SP (10<sup>-6</sup> M), histamine (10 mg ml<sup>-1</sup>), and SLIGRL-NH<sub>2</sub> (100 nM) for 2 hours and harvested. For DNA microarray analysis, total RNA was extracted from Normal human epidermal KCs with the RNeasy Mini Kit (Qiagen, Valencia, CA). Images were analyzed with the DNASIS Array (DNA Chip Research, Hitachi Software Engineering, Tokyo, Japan) according to the manufacturer's instructions. The results of DNA microarray analysis of the top and bottom 20 genes with respect to expression levels induced by SP, histamine, or SLIGRL-NH<sub>2</sub> are shown in the Supplementary Data online.

### Statistical analysis

Data were analyzed using an unpaired Student's *t*-test. *P* < 0.05 was considered to be significant.

### CONFLICT OF INTEREST

The authors state no conflict of interest.

### ACKNOWLEDGMENTS

This study was supported by a grant from the Ministry of Education, Science, Sports and Culture and a grant from the Ministry of Health, Labour and Welfare, Japan. We thank Yukako Miyazaki and Rie Murase for their technical assistance.

### SUPPLEMENTARY MATERIAL

Supplementary material is linked to the online version of the paper at <http://www.nature.com/jid>

### REFERENCES

Agnes RS, Ying J, Kover KE *et al.* (2008) Structure-activity relationships of bifunctional cyclic disulfide peptides based on overlapping pharmacophores at opioid and cholecystokinin receptors. *Peptides* 29:1413–23

- Andoh T, Katsube N, Maruyama M *et al.* (2001) Involvement of leukotriene B(4) in substance P-induced itch-associated response in mice. *J Invest Dermatol* 117:1621–6
- Bonetto V, Jornvall H, Andersson M *et al.* (1999) Isolation and characterization of sulphated and nonsulphated forms of cholecystokinin-58 and their action on gallbladder contraction. *Eur J Biochem* 264:336–40
- Dufresne M, Seva C, Fourmy D (2006) Cholecystokinin and gastrin receptors. *Physiol Rev* 86:805–47
- Harro J (2006) CCK and NPY as anti-anxiety treatment targets: promises, pitfalls, and strategies. *Amino Acids* 31:215–30
- Hossen MA, Sugimoto Y, Kayasuga R *et al.* (2003) Involvement of histamine H3 receptors in scratching behaviour in mast cell-deficient mice. *Br J Dermatol* 149:17–22
- Ikoma A, Steinhoff M, Ständer S *et al.* (2006) The neurobiology of itch. *Nat Rev Neurosci* 7:535–47
- Liu JY, Hu JH, Zhu QG *et al.* (2006) Substance P receptor expression in human skin keratinocytes and fibroblasts. *Br J Dermatol* 155:657–62
- Ma KT, Si JQ, Zhang ZQ *et al.* (2006) Modulatory effect of CCK-8S on GABA-induced depolarization from rat dorsal root ganglion. *Brain Res* 1121:66–75
- Miyasaka K, Ohta M, Kana S *et al.* (2004) Enhanced gastric emptying of a liquid gastric load in mice lacking cholecystokinin-B receptor: a study of CCK-A,B, and AB receptor gene knockout mice. *J Gastroenterol* 39:319–23
- Mollereau C, Roumy M, Zajac JM (2005) Opioid-modulating peptides: mechanisms of action. *Curr Top Med Chem* 5:341–55
- Moriarty P, Dimaline R, Thompson DG *et al.* (1997) Characterization of cholecystokininA and cholecystokininB receptors expressed by vagal afferent neurons. *Neuroscience* 79:905–13
- Morisset J, Julien S, Lainé J (2003) Localization of cholecystokinin receptor subtypes in the endocrine pancreas. *J Histochem Cytochem* 51:1501–13
- Nishijima T, Tokura Y, Imokawa G *et al.* (1997) Altered permeability and disordered cutaneous immunoregulatory function in mice with acute barrier disruption. *J Invest Dermatol* 109:175–82
- Noble F, Wank SA, Crawley JN *et al.* (1999) International union of Pharmacology. XXI. Structure, distribution, and functions of cholecystokinin receptors. *Pharmacol Rev* 51:745–81
- Noguchi J, Kuroda E, Yamashita U (2005) Strain difference of murine bone marrow-derived mast cell functions. *J Leukoc Biol* 78:605–11
- Ohkubo H, Nakanishi S (1991) Molecular characterization of the three tachykinin receptors. *Ann NY Acad Sci* 632:53–62
- Pommier B, Beslot F, Simon A *et al.* (2002) Deletion of CCK2 receptor in mice results in an upregulation of the endogenous opioid system. *J Neurosci* 22:2005–11
- Rehfeld JF, Friis-Hansen L, Goetze JP *et al.* (2007) The biology of cholecystokinin and gastrin peptides. *Curr Top Med Chem* 7:1154–65
- Scholzen T, Armstrong CA, Bunnett NW *et al.* (1998) Neuropeptides in the skin: interactions between the neuroendocrine and the skin immune systems. *Exp Dermatol* 7:81–96
- Steinhoff M, Bienenstock J, Schmelz M *et al.* (2006) Neurophysiological, neurological, and neuroendocrine basis of pruritus. *J Invest Dermatol* 126:1705–18
- Tokunaga Y, Cox KL, Coleman R *et al.* (1993) Characterization of cholecystokinin receptors on the human gall bladder. *Surgery* 113:155–62
- Wiesenfeld-Hallin Z, de Araújo Lucas G, Alster P *et al.* (1999) Cholecystokinin/opioid interactions. *Brain Res* 848:78–89
- Yamada N, Matsushima H, Tagaya Y *et al.* (2003) Generation of a large number of connective tissue type mast cells by culture of murine fetal skin cells. *J Invest Dermatol* 121:1425–32
- Yamaguchi J, Nakamura F, Aihara M *et al.* (2008) Semaphorin3A alleviates skin lesions and scratching behavior in NC/Nga mice, an atopic dermatitis model. *J Invest Dermatol* 128:2842–9
- Yosipovitch G, Papoiu AD (2008) What causes itch in atopic dermatitis? *Curr Allergy Asthma Rep* 8:306–11
- Zheng Y, Akgun E, Harikumar KG *et al.* (2009) Induced association of mu opioid (MOP) and type 2 cholecystokinin (CCK2) receptors by novel bivalent ligands. *J Med Chem* 52:247–58

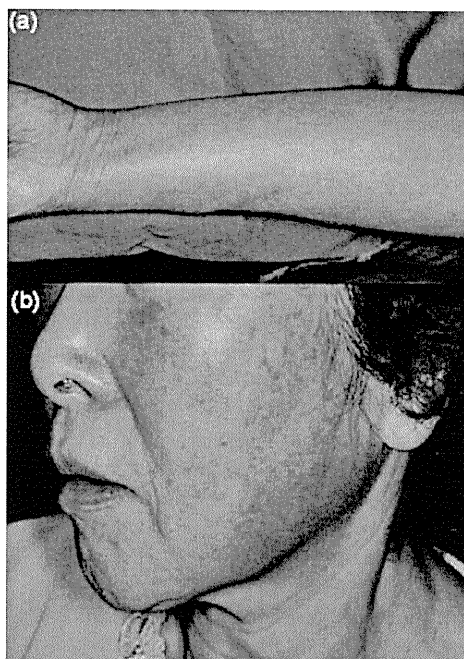


Fig. 1. Recurrent pruritic erythema on the left arm (a) and face (b).

## Occupational contact dermatitis caused by asparagus

Contact Dermatitis 2010; 63: 54–54

Teruki Yanagi<sup>1</sup>, Hiroshi Shimizu<sup>1</sup> and Tadamichi Shimizu<sup>2</sup>

<sup>1</sup>Department of Dermatology, Hokkaido University Graduate School of Medicine, Sapporo, and <sup>2</sup>Department of Dermatology, Toyama University Graduate School of Medicine, Toyama, Japan

**Key words:** asparagus; occupational contact dermatitis; patch test.

### Case Report

A 67-year-old Japanese woman presented with a 2-year history of a recurrent pruritic erythema on the face, arms and hands (Fig. 1). She had worked in an asparagus cannery for 20 years. Her medical history indicated no evidence of atopic disease. The dermatitis cleared quickly with courses of anti-histamines and topical steroids but relapsed within days of returning to work. Rubber gloves were initially of benefit, but the pruritic eruption re-appeared when she touched her face with these gloves after working. She was patch-tested to a metals series and a freshly picked shoot of

*Asparagus officinalis*. At both D2 and D3, the patch test with asparagus showed a strongly positive reaction (++), whereas all metals and white petrolatum were negative. Skin prick test with raw asparagus showed no skin reaction. Three normal healthy volunteer controls were negative on patch testing to asparagus. In light of the clinical observations and test results, occupational contact dermatitis to asparagus was diagnosed.

### Discussion

Asparagus, one of the *Liliaceae* family members, is a vegetable that is cultivated worldwide and consumed when in season. Contact dermatitis to asparagus is rare (1–5). Several cases of allergic reactions by ingestion or inhalation of asparagus have been reported (6). Our patient, working in the cannery, had chronic/seasonally relapsing contact dermatitis to asparagus, which seems to be rare despite the widespread availability and consumption of asparagus. Although an association of contact dermatitis with other *Liliaceae* family members (garlic and onion) has frequently been reported as a result of occupational exposure (7), dermatologists should consider the potential of asparagus as an occupational allergen, particularly if allergic contact dermatitis occurs either chronically or seasonally.

### References

1. Hausen B M, Wolf C. 1,2,3-Trithiane-5-carboxylic acid, a first contact allergen from *Asparagus officinalis* (Liliaceae). *Am J Contact Dermat* 1996; 7: 41–46.
2. Rademaker M, Yung A. Contact dermatitis to *Asparagus officinalis*. *Australas J Dermatol* 2000; 41: 262–263.
3. Rieker J, Ruzicka T, Neumann N J, Bielicky P, Homey B. [Type I and type IV sensitization to *Asparagus officinalis*]. *Hautarzt* 2004; 55: 397–398.
4. Rieker J, Ruzicka T, Neumann N J, Homey B. Protein contact dermatitis to asparagus. *J Allergy Clin Immunol* 2004; 113: 354–355.
5. Tabar A I, Alvarez-Puebla M J, Gomez B et al. Diversity of asparagus allergy: clinical and immunological features. *Clin Exp Allergy* 2004; 34: 131–136.
6. Volz T, Berner D, Weigert C, Rocken M, Biedermann T. Fixed food eruption caused by asparagus. *J Allergy Clin Immunol* 2005; 116: 1390–1392.
7. Hjorth N, Roed-Petersen J. Occupational protein contact dermatitis in food handlers. *Contact Dermatitis* 1976; 2: 28–42.

Address:  
Teruki Yanagi  
Department of Dermatology  
Hokkaido University Graduate School  
of Medicine Sapporo  
Japan  
Tel: +81-11-716-1161  
Fax: +81-11-706-7820  
e-mail: yanagi@med.hokudai.ac.jp





## Modulation of semaphorin 3A expression by calcium concentration and histamine in human keratinocytes and fibroblasts

Shoko Fukamachi<sup>a</sup>, Toshinori Bito<sup>b</sup>, Noriko Shiraishi<sup>a</sup>, Miwa Kobayashi<sup>a</sup>, Kenji Kabashima<sup>c</sup>, Motonobu Nakamura<sup>a</sup>, Yoshiki Tokura<sup>a,\*</sup>

<sup>a</sup> Department of Dermatology, University of Occupational and Environmental Health, Iseigaoka, Yahatanishi-ku, Kitakyushu 807-8555, Japan

<sup>b</sup> Division of Dermatology, Department of Internal Related, Kobe University Graduate School of Medicine, Kobe, Japan

<sup>c</sup> Department of Dermatology, Faculty of Medicine, Kyoto University Graduate School of Medicine, Kyoto, Japan

### ARTICLE INFO

#### Article history:

Received 30 April 2010

Received in revised form 27 October 2010

Accepted 23 November 2010

#### Keywords:

Semaphorin 3A  
Nerve growth factor  
Keratinocyte  
Calcium concentration  
Histamine  
PAR-2

### ABSTRACT

**Background:** Both neurotrophins and chemorepellents are involved in the elongation and sprouting of itch-associated C-fibers in the skin. Nerve growth factor (NGF) and semaphorin 3A (Sema3A) are representatives of these two types of axon-guidance factors, respectively.

**Objective:** We investigated the effects of calcium concentration and histamine on the expression of NGF and Sema3A in normal human epidermal keratinocytes (NHEK) and normal human fibroblasts (NHFB).

**Methods:** NHEK and NHFB were cultured under different calcium concentrations (0.15–0.9 mM) with or without histamine, and the expression of mRNA for NGF and SEMA3A was assessed by real-time PCR analysis. An immunohistochemical study was performed for Sema3A using normal skin and skin cancer specimens.

**Results:** In NHEK, SEMA3A expression was elevated by high calcium concentration and reduced by low calcium condition, while NGF expression was not dependent on calcium. Their expressions were unchanged by calcium in NHFB. Immunohistochemically, keratinocytes in the prickle layer of normal epidermis and squamous cell carcinoma cells were positive for Sema3A, sparing basal cells and suprabasal cells. The addition of histamine to NHEK at 10 µg/ml enhanced SEMA3A expression but depressed NGF expression. In NHFB, however, histamine decreased both NGF and SEMA3A levels.

**Conclusions:** Sema3A inhibits C-fiber elongation/sprouting in the upper layers of the epidermis, where calcium concentration is high, thereby determining the nerve endings. Histamine reduces Sema3A production by fibroblasts, allowing C-fibers to elongate in the dermis. In contrast, the histamine-augmented keratinocyte production of Sema3A might suppress C-fiber elongation and exaggerated pruritus.

© 2010 Japanese Society for Investigative Dermatology. Published by Elsevier Ireland Ltd. All rights reserved.

### 1. Introduction

C-fiber is known as a primary afferent nerve to deliver itch to the central nerve system [1]. Numerical increment and elevated sprouting of C-fiber in the epidermis easily produce itch and accelerate the itch–scratch cycle [2]. In addition, C-fiber plays pluripotential roles for itch-related events. For example, neuropeptides released from C-fibers stimulate keratinocytes and mast cells to produce pruritogenic factors that again stimulate C-fiber [3–5].

Both neurotrophins and chemorepellents regulate the elongation and sprouting of itch-associated C-fibers in the skin. Nerve growth factor (NGF) [6,7] and semaphorin 3A (Sema3A) [8] are representatives of these two types of nerve axon-guidance factors, respectively. NGF and Sema3A have opposite effects on C-fiber elongation, which is related to promotion of itch in the skin. In

atopic dermatitis, the number of peripheral nerve endings is increased and may amplify itch [2]. NGF is known to initiate the sprouting of epidermal nerve fibers in atopic dermatitis and its model NC/Nga mice [9]. Changes in Sema3A expression/production has also been reported in the lesional skin of atopic dermatitis [10,11]. A reduction in Sema3A expression allows nerve fibers to sprout into the upper epidermis, and photochemotherapy may exert a therapeutic effect by increasing epidermal cell production of Sema3A [12]. On the other hands, in normal skin, the extracellular calcium concentration critically determines a variety of biological activities of keratinocytes [13]. The calcium concentration increases towards the outer epidermis, forming a “calcium gradient” within the epidermis [14]. It is possible that this physiological condition influences on the production of the nerve guidance factors. In addition, histamine released from mast cells in certain allergic conditions possibly modulates their production.

To address the regulatory mechanisms underlying C-fiber elongation, we investigated the effects of calcium concentration on the expression of NGF and SEMA3A in normal human epidermal keratinocytes (NHEK). Upon allergic stimulation, histamine and

\* Corresponding author. Tel.: +81 93 691 7445; fax: +81 93 691 0907.  
E-mail addresses: [tokura@med.uoeh-u.ac.jp](mailto:tokura@med.uoeh-u.ac.jp), [jsid@mbox.med.uoeh-u.ac.jp](mailto:jsid@mbox.med.uoeh-u.ac.jp)  
(Y. Tokura).

tryptase are produced by mast cells, and keratinocytes express H1 receptors for histamine and protease-activated receptor-2 (PAR-2) for tryptase [15,16]. Therefore, it is an interesting issue to investigate the effects of histamine and a PAR-2 agonist, SLIGRL-NH<sub>2</sub> (SLIGRL) on the expression of these guidance factors in NHEK and normal human fibroblasts (NHFB). Results suggest that the physiological and pathological conditions of the skin modulate the production of NGF and Sema3A by keratinocytes and fibroblasts.

## 2. Material and methods

### 2.1. Chemicals

Histamine and a PAR-2 agonist SLIGRL were purchased from Wako (Osaka, Japan) and Tocris (Ellisville, MO), respectively. These substances were freshly diluted by distilled water before use.

### 2.2. Cell and cell culture

Primary culture of NHEK was obtained from Lonza (Basel, Switzerland). NHEK were grown in Keratinocyte Growth Medium-2 (KGM-2) for expansion and Keratinocyte Basal Medium-2 (KBM-2; Lonza) for experiments at 37 °C in a 5% CO<sub>2</sub> atmosphere. Primary NHFB were obtained from Takara (Osaka, Japan) and cultured in Dulbecco's Minimum Essential Medium (DMEM) supplemented with 10% fetal bovine serum, 100 U/ml penicillin, 100 µg/ml streptomycin and 2 mM glutamine.

### 2.3. Real-time quantitative reverse transcription-polymerase chain reaction (RT-PCR) analysis

NHEK were grown to subconfluence in KGM-2, unstimulated or stimulated with histamine or SLIGRL under various calcium concentration in KBM-2, and then harvested. cDNA was synthesized directly from cell lysate solution using TaqMan Gene Expression Cells-to-CTM Kit (Austin, TX) according to manufacturer's instructions. The conditions of reverse transcription were as follows: 60 min at 37 °C, 5 min at 95 °C, and then hold at 4 °C. Amplification reaction was performed using ABI PRISM 7000 Sequence Detection System (Applied Biosystems; Carlsbad, CA) with TaqMan Gene Expression Assays (Applied Biosystems). Primers and TaqMan probe for human *SEMA3A* and human *NGF* were purchased from Applied Biosystems. Amplification of human  $\beta$ -actin, *ACTB* (TaqMan  $\beta$ -actin Control-Reagent Kit) was used as an endogenous control for quantification. The conditions of the real-time PCR were as follows: 2.0 min at 50 °C (reverse transcription), 10 min at 95 °C (RT inactivation and initial activation), and then 40 cycles of amplification consisting of 15 s at 95 °C (denaturation) and 1 min at 60 °C (annealing and extension). All heating and cooling steps were performed with a slope of 20 °C/s. Samples were analyzed in triplicates and averages were calculated for analysis of the expression ratios.

### 2.4. Western blotting

NHEK were cultured at 0.15 mM or 0.6 mM of calcium concentration in 6-well plates for 12 h, harvested with rubber policeman, and subjected to extraction by RIPA buffer (50 mM Tris-HCl [pH8.0], 150 mM sodium chloride, 0.5 w/v% sodium deoxycholate, 0.1 w/v% sodium dodecyl sulfate, and 1.0 w/v% NP-40 substitute; Wako Chemical Co., Tokyo, Japan). Ten µg protein samples were electrophoresed by 8% SDS-polyacrylamide gel electrophoresis and electroblotted onto polyvinylidene difluoride membranes for 2 h at 180 mA. After blocking with 5% skim milk solution, the membranes were incubated with rabbit anti-human Sema3A (sc-28867; 1:1000, Santa Cruz Co., Santa Cruz, CA), NGF

(sc-548; 1:1000), or Loricrin (PRB-145P; 1:1000, Covance, NJ) polyclonal antibodies, and the reaction was detected with horseradish peroxidase-conjugated goat anti-rabbit IgG (1:3000, Bio-Rad, Hercules, CA). Immunoblots were visualized using the ECL Plus Western Blotting Detection Reagents (GE Healthcare, Buckinghamshire, England) according to the manufacturer's protocol.

### 2.5. Cytometric beads array

IL-8 and GM-CSF concentration in the culture supernatants were determined with Cytometric Bead Array (CBA) Flex Set System purchased from Becton Dickinson and Company (Franklin Lakes, NJ) using FACSCanto (Becton Dickinson).

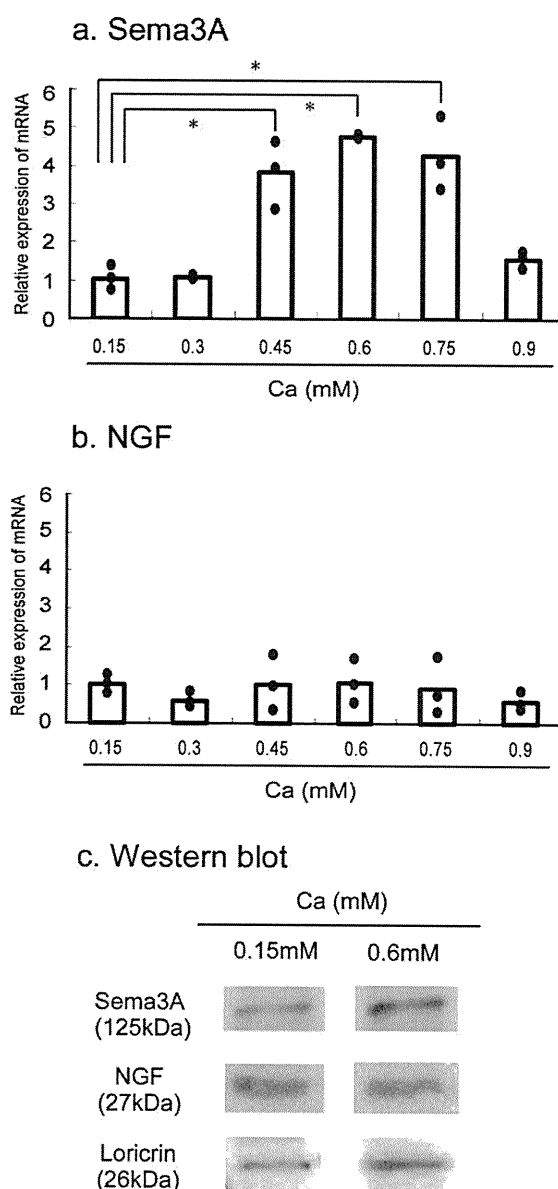


**Fig. 1.** Effects of calcium concentration on the expression of *SEMA3A* and *NGF* in NHEK. NHEK were cultured under varying concentrations, ranging from 0.15 to 0.9 mM for 2 h. After harvesting, cDNA was synthesized directly and the expression of *SEMA3A* (a) and *NGF* (b) was assessed by real-time PCR. The data are expressed as (expression level of 0.3–0.9 mM calcium group)/(expression level of 0.15 mM calcium group). Bars represent the means of three independent experiments. \**P* < 0.05. The expression levels of Sema3A, NGF, and loricrin in NHEK cultured under 0.15 or 0.6 mM calcium were analyzed by Western blotting (c).

## 2.6. Immunohistochemistry

Formalin-fixed and paraffin-embedded 4- $\mu$ m sections of specimens were deparaffinized and rehydrated through descending alcohol series and in phosphate buffered saline (PBS, pH 7.4). Antigen was retrieved with Antigen Retrieval Citra (BioGenex Laboratories, San Ramon, CA), and endogenous peroxidase was quenched with 1.5% hydrogen peroxide in methanol. After blocking nonspecific antigen binding sites with 3% nonimmune serum, anti-Sema3A rabbit polyclonal IgG antibodies (sc-28867; 1:200; Santa Cruz) was applied overnight at 4 °C. After rinsing with PBS, sections were incubated with biotinylated secondary antibody and then with peroxidase conjugated avidin solution (Vector Laboratories Inc., Burlingame, CA). Peroxidase was visualized with 3-amino-9-ethylcarbazole chromogen, and the sections were lightly counterstained with hematoxylin.

## 2.7. Statistical analysis

Data were analyzed using an unpaired two-tailed *t*-test. *P*-value of less than 0.05 was considered to be significant.

## 3. Results

### 3.1. High calcium augments the expression of SEMA3A but not NGF in NHEK

Keratinocytes proliferate at a low calcium concentration, such as 0.15 mM, and differentiate at a high calcium concentration in culture [12]. The proliferating and differentiating cells represent

the basal cell in the lower most epidermis and the prickle cell in the upper epidermis, respectively. To address the physiological production of Sema3A and NGF by epidermal keratinocytes, NHEK were cultured under varying calcium concentrations, ranging from 0.15 to 0.9 mM, and after 2-h incubation, the expression of *SEMA3A* and *NGF* was assessed by real-time PCR. Whereas *SEMA3A* expression was low at 0.15 or 0.3 mM calcium, its expression was upregulated at higher concentrations of 0.45–0.75 mM (Fig. 1a). Calcium at 0.9 mM or more reduced the expression of *SEMA3A*. In contrast, calcium concentration did not affect the expression of *NGF* in NHEK (Fig. 1b). The incubation period of 24 h produced the comparable levels of *SEMA3A* and *NGF* expression to the 2-h incubation.

To confirm the above finding at the protein level, we performed a Western blot analysis for Sema3A, NGF, and differentiation marker loricrin in NHEK cultured with 0.15 or 0.6 mM calcium. NHEK incubated with 0.6 mM calcium showed higher levels of Sema3A as well as loricrin than those with 0.15 mM calcium, while the levels of NGF were comparable between them (Fig. 1c). These results indicate that the production of Sema3A but not NGF is dependent on calcium concentration.

### 3.2. Immunohistochemical staining for Sema3A in normal skin and cutaneous tumors

The above finding suggested that Sema3A is highly expressed in the upper epidermis where keratinocytes are differentiated by high calcium concentration. We therefore investigated Sema3A expression by immunohistochemistry in normal skin, squamous cell carcinoma (SCC), and basal cell carcinoma (BCC). In normal

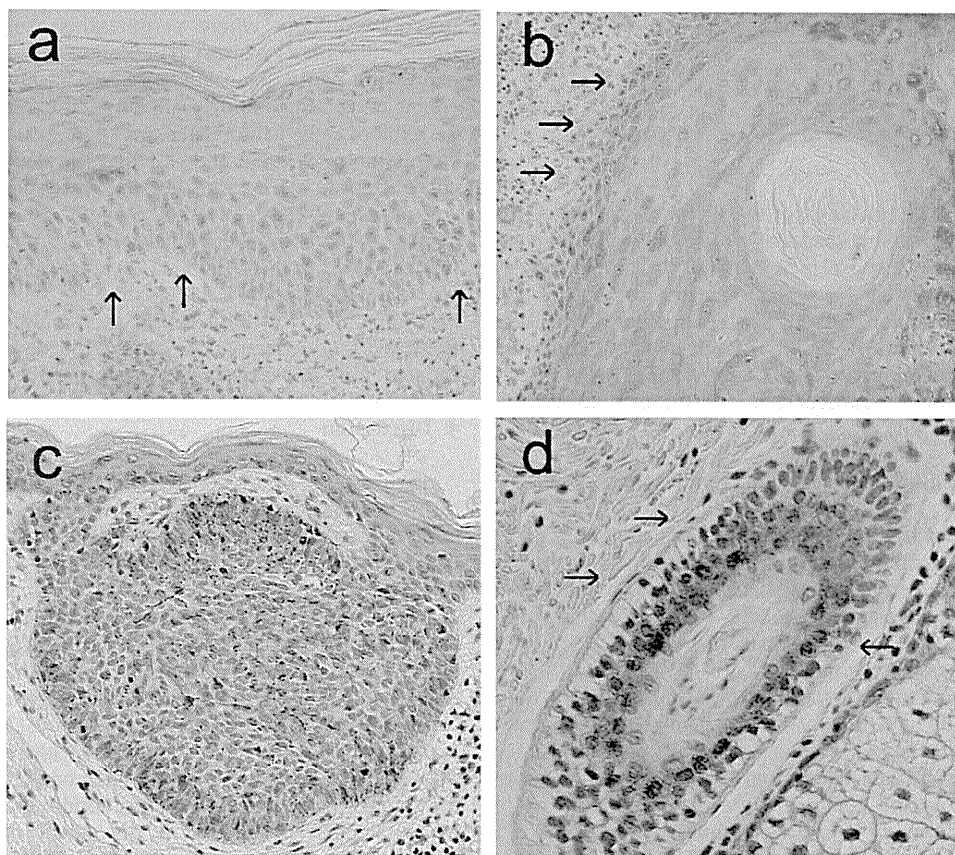


**Fig. 2.** Sema3A expression in normal skin and SCC. Immunohistochemical staining for Sema3A in normal epidermis (a), tumor nest of SCC (b), tumor nest of BCC (c), and hair follicle (d). Arrows indicate basal and suprabasal cells stained negatively. Original magnification:  $\times 200$ .

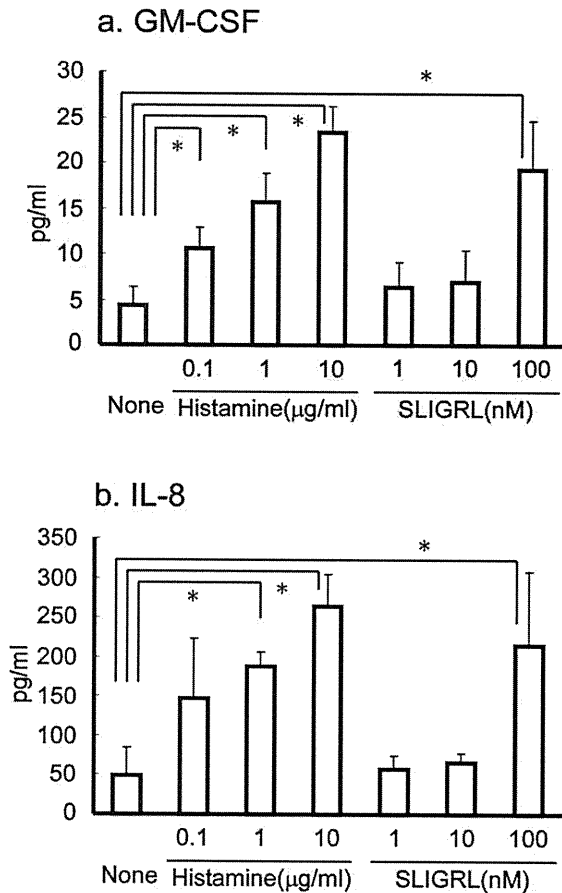


**Fig. 3.** Effects of histamine and SLIGRL on cytokine/chemokine production by NHEK. NHEK were cultured with various concentrations of histamine or SLIGRL for 48 h. The amounts of IL-8 and GM-CSF in the supernatants was measured using CBA. Bars represent the means  $\pm$  SD of IL-8/GM-CSF concentration in triplicate. \* $P < 0.05$ .

skin, keratinocytes of the prickle layer were positive for Sema3A, while cells of the basal and suprabasal layers and the granular layer were negative (Fig. 2a). Likewise, in SCC tissues, squamoid tumor cells were strongly positive for Sema3A except for basal and suprabasal cells of the tumor nests (Fig. 2b). The epidermal cells of BCC were negative for Sema3A (Fig. 2c). In hair follicles of normal skin, inner cells in the outer root sheath were strongly Sema3A-positive, but basal and suprabasal cells in this part were not positively stained (Fig. 2d).

### 3.3. Histamine and SLIGRL are bioactive for keratinocytes

Since histamine is one of the critical pruritus-related molecules involved in allergic skin disorders, we examined its effect on Sema3A and NGF production by keratinocytes. SLIGRL was also tested in parallel, because signaling via PAR-2 is important as well as signaling via H1 receptor in C-fiber stimulation [15], and keratinocytes express both the receptors [16,17].

In advance of testing the effects of histamine and SLIGRL on the production of Sema3A and NGF, we confirmed their biological activities on keratinocytes and estimated their optimal concentrations in our culture system. NHEK were cultured at 0.15 mM calcium with histamine (0.1–100  $\mu$ g/ml) and SLIGRL (1–1000 nM) for 48 h. In our preliminary study, we examined the effects of histamine and SLIGRL on the production by NHEK of GM-CSF, IL-8, CXCL9/MIG, CXCL10/IP-10, CCL5/RANTES, CCL22/MDC, and vascular endothelial growth factor. Among these cytokines and

chemokines, GM-CSF and IL-8 were increased by histamine and SLIGRL. We therefore chose these two cytokines in the following experiments. When these two cytokines were quantified in the supernatants, histamine at 0.1  $\mu$ g/ml or more and SLIGRL at 100 nM increased the production of GM-CSF and IL-8 by NHEK (Fig. 3). Histamine 100  $\mu$ g/ml and SLIGRL 1000 nM were toxic to NHEK as they abolished cell viability (data not shown). Therefore, histamine at 10  $\mu$ g/ml and SLIGRL 100 nM were used in the following studies.

### 3.4. Histamine upmodulates SEMA3A expression and downmodulates NGF expression in keratinocytes

Incubation of NHEK with histamine (10  $\mu$ g/ml) for 2 h upregulated the expression of SEMA3A under either 0.15 mM or 0.6 mM of calcium concentration, while stimulation with SLIGRL (100 nM) unaffected SEMA3A expression at both calcium concentrations (Fig. 4a). SLIGRL at higher concentrations (up to 10  $\mu$ M) was also tested, but SEMA3A expression was not increased (data not shown). On the contrary, the expression of NGF was significantly decreased by histamine at 10  $\mu$ g/ml or SLIGRL at 100 nM, although the former's suppressive activity was higher than the latter's (Fig. 4b). Thus, histamine but not SLIGRL augmented the expression of Sema3A, and both stimulants inhibited NGF expression in keratinocytes. Thus, the opposite effects of histamine on Sema3A and NGF productions are remarkable.

### 3.5. Histamine and SLIGRL downregulate the expression of both SEMA3A and NGF in fibroblasts

In addition to the epidermis, the dermis is a critical microenvironment where peripheral sensory nerve elongates. Dermal fibroblasts express H1 receptor [18] and PAR-2 [19]. The expression of the axon guidance factors by fibroblasts and the effects of histamine and SLIGRL on their expressions are issues to be explored. By using NHFb, we first examined the fibroblast expression of SEMA3A and NGF and the dependency on calcium concentration. NHFb expressed mRNAs for both factors, and there was no modulatory effect of calcium concentration (data not shown). Next, NHFb were incubated with histamine (1 or 10  $\mu$ g/ml) or SLIGRL (10 or 100 nM) for 2 h. The expression levels of SEMA3A (Fig. 5a) and NGF (Fig. 5b) were significantly reduced by histamine at 10  $\mu$ g/ml or SLIGRL at 100 nM, suggesting that the fibroblast production of both axon guidance factors with opposite capacities are depressed by these mast cell-released mediators.

## 4. Discussion

In this study, we demonstrated the modulation of SEMA3A and NGF expressions by calcium concentration and histamine or SLIGRL. The expression of SEMA3A depended on calcium concentration in NHEK, but not in NHFb. Whereas NHEK cultured at low calcium concentrations of 0.15–0.3 mM, inducible for keratinocyte proliferation, expressed low levels of SEMA3A, cells cultured at high calcium concentrations of 0.45–0.75 mM, suitable for keratinocyte differentiation, expressed high levels of SEMA3A. On the contrary, NGF was constitutively expressed by NHEK irrespective of calcium concentration. Therefore, the expression of SEMA3A but not NGF is markedly regulated by calcium concentration in epidermal keratinocytes, implying that the chemorepellent may control C-fiber elongation in the physiological condition. The mechanisms by which Sema3A production is dependent on the extracellular calcium concentration is not clear. One possible explanation is that  $Ca^{2+}$  signaling participates in the transcription of Sema3A gene. The second messenger inositol triphosphate and intracellular